

Putting Fair Division on the Map

Paula Böhm

Institut für Informatik
TU Clausthal
Clausthal-Zellerfeld, Germany
FIXME@tu-clausthal.de

Robert Brederick

Institut für Informatik
TU Clausthal
Clausthal-Zellerfeld, Germany
robert.brederick@tu-clausthal.de

Paul Gözl

ORIE
Cornell University
Ithaca, NY, USA
paulgoelz@cornell.edu

Andrzej Kaczmarczyk

Department of Computer Science
The University of Chicago
Chicago, IL, USA
akaczmarczyk@uchicago.edu

Stanisław Szufa

CNRS, LAMSADE
Université Paris Dauphine - PSL
Paris, France
s.szufa@gmail.com

Abstract

The fair division of indivisible goods is not only a subject of theoretical research, but also an important problem in practice, with solutions being offered on several online platforms. Little is known, however, about the characteristics of real-world allocation instances and how they compare to synthetic instances. Using dimensionality reduction, we compute a *map* of allocation instances: a 2-dimensional embedding such that an instance's location on the map is predictive of the instance's origin and other key instance features. Because the axes of this map closely align with the utility matrix's two largest singular values, we define a second, explicit map, which we theoretically characterize.

1 Introduction

Over the past 20 years, the field of fair division has made great advances in studying allocations of indivisible goods [Amanatidis et al., 2023]. To illustrate this progress, consider the axiom of *envy-freeness*, which demands that no agent prefer another agent's bundle of allocated goods to their own. By the end of the 20th century, economists already understood envy-freeness well in settings with *divisible* goods. For example — assuming that preferences are additive, as we do throughout the paper — the allocation maximizing the Nash welfare is envy-free in these settings [Varian, 1974, Shafer and Sonnenschein, 1982]. Little was known, however, about indivisible goods, a domain whose combinatorial structure poses additional challenges to mathematical investigation. Since envy-free allocations need not exist for all indivisible allocation instances¹, could envy at least be limited, or were large amounts of envy unavoidable?

¹Under the standard assumption that all goods must be allocated, which we also make throughout the paper.

Since then, we have gained a refined understanding of the degree to which envy can (and cannot) be avoided. Notably, the field has coalesced around an attractive relaxation of envy-freeness — *envy-freeness up to one good (EF1)* [Budish, 2011] — and identified elegant algorithms [Lipton et al., 2004, Caragiannis et al., 2019] that construct EF1 allocations for any instance. Though intriguing open questions remain,² these questions sharpen and extend a solid understanding of the landscape of allocations. For alternative families of fairness axioms (such as the maximin share, proportionality, and equitability), fair division has made similar progress in understanding which axioms can be guaranteed even on worst-case allocation instances [Amanatidis et al., 2023].

In parallel to these theoretical advances, algorithms for allocating indivisible goods have entered practical usage, raising new questions for fair division. The Course Match system, for example, assigns course seats to MBA students at Wharton [Budish et al., 2017], and thousands of users have used the website Spliddit [Goldman and Procaccia, 2014] to divide up estates or joint possessions. The deployment of such systems makes it more pressing to study not only worst-case instances but instances typically encountered in practice as well. For example, though envy-free allocations do not exist for all instances, should algorithms not aim for envy-free allocations for the 71% of Spliddit instances [Bai et al., 2022] where envy-freeness is possible? If so, how to choose among envy-free allocations? Or, as a second example, which algorithms can be implemented in practice? After all, the algorithms deployed on Course Match [Budish et al., 2023] and Spliddit [Caragiannis et al., 2019], as well as other proposed methods [Bredereck et al., 2021], run fast on practical inputs seemingly defying (worst-case) computational hardness results. Answers to these questions cannot be found through worst-case analysis alone.

Whereas most work in fair division follows the worst-case paradigm, a noteworthy exception is some work in the paradigm of *distributional analysis*, which assumes that allocation instances are drawn from a probability distribution [Roughgarden, 2020]. Typically, these distributional models assume that all agent–good values are drawn independently, either from a single distribution [Amanatidis et al., 2017, Manurangsi and Suksompong, 2019, 2021], a distribution that depends on the agent [Kurokawa et al., 2016, Farhadi et al., 2019, Bai and Gözl, 2022], or a distribution that depends on the alternative [Dickerson et al., 2014, Farhadi et al., 2019].

On the upside, when m and n are large, these distributions generate highly structured instances, for which fair allocations are more prevalent. For example, basic algorithms yield envy-free allocations for these instances, with high probability [Dickerson et al., 2014, Manurangsi and Suksompong, 2021]. On the flip side, we are not aware of any empirical work that has tested if the structures of these random instances are present in practical allocation problems.³ In recent work, Bai et al. [2022] try to overcome some of these concerns through *smoothed analysis*, which means that their probability distributions are defined by adding random noise to a worst-case utility profile. While they extend the possibility results for envy-freeness to more general distributions, they leave “whether our smoothed model accurately describes the properties of real-world utility profiles that possess envy-free allocations” to future empirical analysis.

Recently, social choice theory addressed a similar need for bridging the gap between theoretical work and practical instances. Famously riddled with worst-case impossibilities [Campbell and Kelly, 2002], modern social choice theory has been largely divorced from the analysis of election data. Part of the theory considered distributional models of elections, but these models were overly prescriptive and, anyway, not easy to relate to real-world elections. To address these concerns, Szufa et al. [2020] created a *map of elections*: A two-dimensional embedding of election instances (originally from distributional models and, in subsequent work [Boehmer et al., 2021, Faliszewski et al., 2023], also from real-world data) with the following properties:

²For example, whether envy-freeness up to *any* good (EFX) can be guaranteed [Chaudhury et al., 2020, Plaut and Roughgarden, 2020, Amanatidis et al., 2021].

³Bai et al. [2022] voice doubts, but also do not provide data.

- This map recovers tell-tale features of the different data sources, turning elections generated by a specific probability distribution into a compact cluster, which evidently only covers a small subset of interesting elections.
- Key features of election instances vary continuously over the map, showing that an election’s position on the map is highly informative — despite rendering the high-dimensional space of elections in just two dimensions.
- The map’s two axes can be given a conceptual interpretation, and the boundary of the map be traced by natural “extreme” elections.

One achievement of this line of work was to highlight distributional models which, at least on the axes of the map, capture the range of interesting elections. We apply a similar approach to fair division.

1.1 Our Approach and Results

In fact, we create *two* maps of allocation instances for indivisible goods in this paper. In Section 3, we create a map by following the methodology of Szufa et al. [2020]: we define a natural distance between fair division instances (the ℓ^1 distance between utility matrices up to row and column permutations), and use multi-dimensional scaling [Kruskal, 1964] (a common technique for dimensionality reduction) to find a 2-dimensional *distance-embedding map* of a given set of allocation instances that approximately preserves the pairwise distances. To scale this approach to allocation instances with many agents and goods, we also propose a computationally tractable proxy distance, which leads to almost identical maps at a much smaller computational cost.

Using data from three real-world data sources and several synthetic distributions over approval instances, we show that the map picks up on common properties of instances from the same data source. We also show that key features of the allocation instance (e.g., the maximum achievable Nash welfare or the existence of envy-free allocations) are distributed in clear patterns across the map. Whereas two natural probability distributions over instances fail to cover the whole range of real-world instances, a new distribution we propose covers the whole map in our experiments and is therefore a natural choice for future synthetic experiments in fair division.

In Section 4, we go beyond the heuristically generated embedding described above, by providing an *explicit map*, i.e., an explicit function from allocation instances into \mathbb{R}^2 , which reproduces the general layout of the distance-embedding map. Since an instance’s position on this explicit map is given by the two largest singular values of its utility matrix, our explicit map is amenable to theoretical analysis. In particular, we tightly characterize the range of the map, and identify (up to rounding terms) the most extreme instances in the map’s four corners. We conclude by showing that the explicit map can similarly segment instance sources and features.

2 Preliminaries

Let $[n]$ be a set of agents and $[m]$ be a set of goods. For ease of exposition, we assume throughout the paper that $m \geq n \geq 2$, which arguably includes all interesting allocation instances. An *allocation instance* (of indivisible goods) is described by a *utility matrix* $U \in \mathbb{R}_{\geq 0}^{n \times m}$ whose entries $u_{i,j}$ describe agent i ’s utility for good j . We refer to the i th row of this matrix as i ’s *utility vector* $\vec{u}_i \in \mathbb{R}_{\geq 0}^m$. We assume that preferences are additive, so that agent i ’s utility for a *bundle* $S \subseteq [m]$ of goods is given by $u_i(S) := \sum_{j \in S} u_{i,j}$. Since we only consider tasks in which agents’ utilities $u_i([m])$ for the whole bundle are normalized to 1, we consider exactly the set of *row-stochastic* matrices U .

2.1 Characteristic Instances

As useful signposts for navigating through the space of allocation instances, we define several *characteristic instances*. Each of these instances represents an intuitively extreme scenario with easily-understood, symmetric structure. Due to space limitations, we introduce these instances in words here, and refer the reader to Fig. 6 in the appendix for a matrix representation. For any n and m , our three characteristic instances are the following:

Indifference (IND) models the situation where each good is equally valuable to each agent.

Thus, all entries of its utility matrix are $1/m$.

Separability (SEP) captures the scenario in which each agent values exactly one good, distinct from the goods that all other agents value. Thus, its utility matrix is a matrix with ones on the diagonal and zeros everywhere else. In particular, if $m > n$, all but the first n columns have all-zero entries.

Contention (CON) considers one single good valued by all agents, and all other goods yielding no value to any agent. Hence, its utility matrix has a first column of ones, and is zero everywhere else.

In Section 4.2, the explicit map will lead us to introduce three new characteristic instances: two variants of separability and an entirely new instance called *bicontention*.

2.2 Real-World Instances

Three of the instance sources we consider generate instances derived from real-world preferences over goods. Two of these sources have not been previously analyzed in the fair-division literature:

Spliddit. The heart of our real-world data is a dataset [Shah, 2022] of all allocation instances submitted to Spliddit as of 2022. This dataset is particularly valuable because it represents instances that real Spliddit users were hoping to solve. Since most of the 3000 Spliddit instances are small, our evaluation will focus on two combinations of n , m that are relatively well represented: First, we will study the setting $n = 3, m = 6$, for which the number of instances (namely, 1847) is highest. Since, for larger dimensions, the number of Spliddit instances drops precipitously, only 16 Spliddit instances exist for our second evaluation scenario of $n = m = 5$.

Island. To obtain this dataset [Benadè, 2023], Benadè et al. [2018] elicited additive utilities for private goods (though they were motivated by a public-goods setting), by asking 572 crowd workers to spread 100 points between 10 items in proportion to how much they would value these items (a map, pocket knife, compass, etc.) if they were stranded on a deserted island. By sampling sets of n agents and m goods and rescaling agents' utilities, we simulate (hypothetical) allocation scenarios in which only those m goods stand to be allocated between those n (real but fictitiously stranded) agents.

Candy. Our final dataset [Anonymized, 2023] has a similar shape and consists of the additive preferences over 10 types of snacks indicated by 48 teenagers attending a summer camp. We again obtain instances by subsampling, assuming that only one snack of each type is available.

2.3 Distributions over Synthetic Instances

In addition to the above instances derived from practical data, we consider synthetic instances drawn from three types of distributions:

I.i.d. As described in the introduction, i.i.d. valuations have been empirically and theoretically studied in the literature. Each agent i 's utility vector is independently generated by sampling i 's values for the m goods independently from some fixed distribution \mathcal{D} , and then rescaling this vector to sum up to 1. In our experiments, we choose \mathcal{D} as the uniform distribution over $[0, 1]$ and as the exponential distribution. (The exponential distribution's rate is inconsequential since utilities are normalized.)

Attributes. This describes a natural explanatory model of how agents’ utilities arise (also used by Boehmer et al. [2023]). Let $d \in \mathbb{N}$ be a fixed number of *attributes*. For each good j , we sample a vector \vec{g}_j from $[0, 1]^d$ uniformly at random (higher coordinates indicate that the good is more desirable along an attribute). For each agent i , we sample a *priority vector* \vec{a}_i over the attributes also from $[0, 1]^d$ (higher coordinates indicate that the agent cares more about an attribute). Then, agent i ’s utility for good j is proportional to the dot product of \vec{a}_i and \vec{g}_j .

Resampling. The former two distributions will end up only covering small areas of the map. Hence, we introduce a third distribution, inspired by that over approval elections [Szufa et al., 2022], which will cover the range of real-world allocation instances. For each agent, we generate a set of *approved* goods over which the agent splits the total utility of 1 equally. Given two parameters $p \in [0, 1]$ and $\phi \in [0, 1]$, we first choose the instance’s *central approval set* V^* by uniformly drawing $\lfloor p \cdot m \rfloor$ goods. Then, we determine whether agent i approves a good j as follows (independently across i, j): with probability $1 - \phi$, i approves j iff $j \in V^*$; else, i approves j with probability p . Should this process leave i without any approved goods, they approve one good uniformly at random.

3 Distance-Embedding Map

We create our first map by performing the following two steps, introduced by Szufa et al. [2020]. First, we define a notion of distance between pairs of allocation instances, and compute all pairwise distances for a collection of instances from the sources described above.⁴ Second, we use *multi-dimensional scaling* [Kruskal, 1964] to embed this collection of instances into the plane in a way that approximately preserves their pairwise distances, which will allow us to see patterns in the similarity of instances.

3.1 Distances between Allocation Instances

Naïvely, we would like to measure the distance between two instances (with equal n and m) through the entry-wise ℓ^1 norm. That is, if the instances’ utility matrices are U^1 and U^2 , we would calculate their distance $\|U^1 - U^2\|_{1,1}$ by summing up, over all $n \cdot m$ coordinates, the absolute difference between U^1 ’s and U^2 ’s entry at this coordinate. This distance is, however, not desirable, since the ordering of rows and columns in a utility matrix is arbitrary but would greatly impact this distance. Instead, an appropriate distance between allocation instances ought to remain invariant when reordering the utility matrices’ rows (i.e., agents) or columns (i.e., goods).

Our *valuation distance* achieves these goals of anonymity and neutrality by explicitly minimizing over all row and column permutations. To express this without matrix notation, suppose that we have bijections $\pi_{agents} : [1, n] \rightarrow [1, n]$ and $\pi_{goods} : [1, m] \rightarrow [1, m]$ between, respectively, the agents and the goods of the first and second allocation instance. By summing up, for each agent i and each good j , the absolute difference $|U_{i,j}^1 - U_{\pi_{agents}(i), \pi_{goods}(j)}^2|$ between i ’s utility for j and the utility of i ’s matched agent $\pi_{agents}(i)$ for j ’s matched good $\pi_{goods}(j)$, we calculate the entry-wise ℓ^1 distance; the valuation distance is defined as the minimum of this distance, taken over all matchings π_{agents} and π_{goods} . A nice property of the valuation distance is that two instances U^1 and U^2 have distance zero exactly if they are identical up to relabeling agents and goods, i.e., they are *isomorphic*.

The valuation distance confirms our intuition that the characteristic instances introduced in Section 2.1 are indeed “extreme points” in the space of allocation instances in the sense that, if $n = m$, the characteristic instances are mutually equidistant at distance $2(m - 1)$; and this distance is maximal (see Proposition 1 in Appendix B.2).

⁴Appendix A describes the number and parameters of the instances we study from each source.

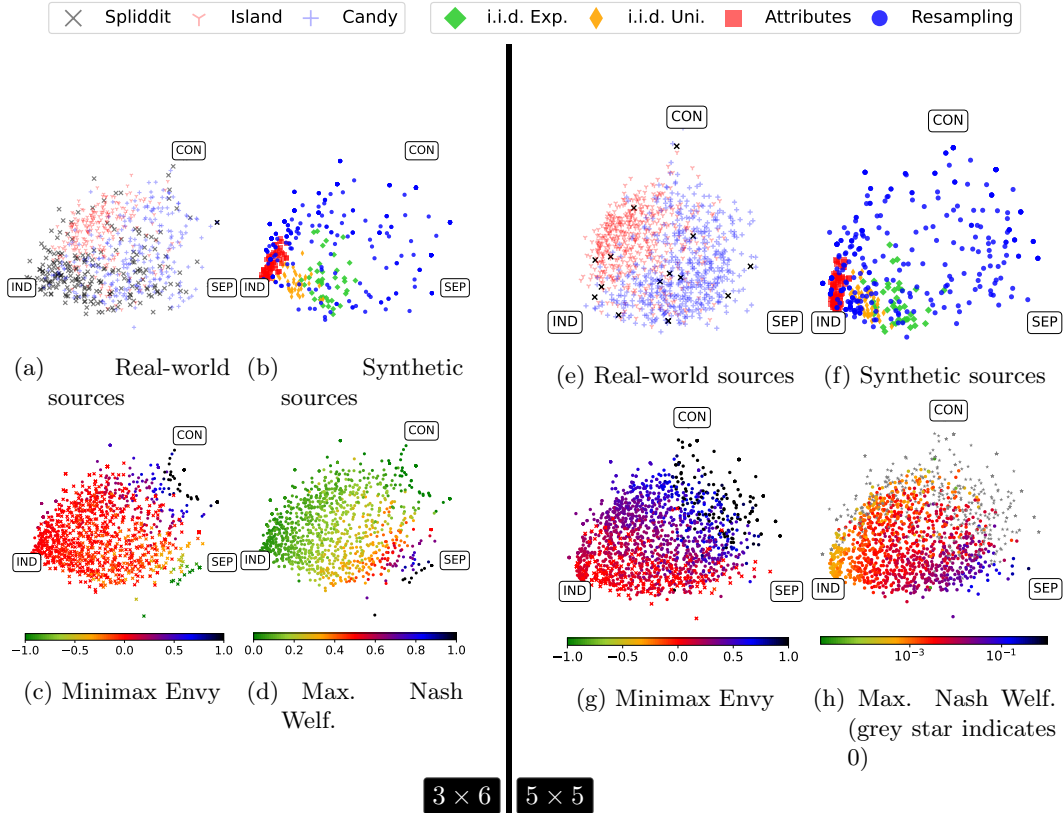


Figure 1: Distribution of instance sources and two features on the distance-embedding maps.

3.2 Studying the Distance-Embedding Map

To plot distance-embedding maps, we first generate a collection of instances from all of our sources — as mentioned in Section 2.2, we consider two combinations of n, m : for $n = 3, m = 6$ (“ 3×6 ” from now on) and for $n = m = 5$ (“ 5×5 ”); see Appendix A.1 for details. Then, we compute the valuation distance between all pairs of instances in each collection, and embed the distances in 2D Euclidean space using multi-dimensional scaling (implemented in scikit-learn, using default parameters).⁵ Fig. 1 displays the resulting embeddings, where each point represents an instance, and an instance’s location stays fixed within all maps of the same dimension. Note that the characteristic instances lie in distinct corners of the map, reflecting our observation at the end of the previous subsection. Most of the map is spanned in a triangle between these three instances, making them useful points of reference.

We can also immediately make out that the instance sources are spread in different patterns across the map. Among the real-world sources (Figs. 1a and 1e), the Spliddit instances are concentrated near indifference for 3×6 instances but spread evenly across the map among 5×5 instances. The island instances tend to vary between indifference and contention whereas the candy instances tend to lie closer to separability, which suggests that the agents’ preferences over survival items are more aligned than the children’s preferences over snacks. Among the synthetic distributions (Figs. 1b and 1f), the i.i.d. distributions and attributes model generate concentrated clusters close to indifference (Figures 21 to 27 in Appendix D display each distribution separately). The observation that these synthetic distributions do not cover the range of the real-world data (and even of just the Spliddit data)

⁵We implemented the generation of our distance-embedding maps as a module of *mapel* (<https://mapel.simple.ink>), a framework for computing maps of elections [Szufa et al., 2020], and will release this module as open source.

raises concerns about the degree to which distributional-analysis results for i.i.d. instances (or attributes instances) can be applied to real-world fair division problems. Since the resampling instances cover the map to a much higher degree, the resampling distribution appears to be a more fruitful proxy for real-world instances for future studies.⁶

Next, we discuss how several natural features of allocation instances vary across the map, which we compute using constraint programming. In Figs. 1c and 1g, we study to which degree the instances allow for (almost) envy-free allocations. Specifically, denote an allocation of all goods over the agents by $[m] = S_1 \dot{\cup} S_2 \dot{\cup} \dots \dot{\cup} S_n$, where S_i denotes agent i 's bundle. The *minimax envy* is the minimum, over all allocations, of the largest amount by which some agent envies another, i.e., $\max_{i \neq i'} u_i(S_{i'}) - u_i(S_i)$. An instance has envy-free allocations if and only if the minimax envy is at most 0 (we highlight these instances with cross markers). But the minimax envy gives a gradual measure of how far envy-freeness is from being achievable (or how much it can be overattained). As we can see, an instance's position on the map is highly informative for the minimax envy and the existence of envy-free allocations. For 3×6 instances, envy-freeness seems to be hopeless near contention (which is also the case for contention itself) and easy near separability. For the rest of the map, minimax envy is close to zero, which means that almost envy-free allocations exist widely, and exactly envy-free allocations generally exist below the upper outline of the map. 5×5 instances are less hospitable to envy-freeness: envy-free allocations exist only near the lower border of the map, and the minimax envy becomes higher (i.e., worse), the further up on the map an instance lies.

Finally, Figs. 1d and 1h show that the maximum Nash welfare achievable by any allocation also varies smoothly over the map, increasing the closer an instance lies to separability. It is noteworthy that this map differs only slightly from the maximum utilitarian welfare that can be achieved (see Fig. 2b below). We show the distribution of various additional features in Appendix D.

3.3 A Faster Distance for Large Instances

Creating these distance-embedding maps required computing the valuation distance for many pairs of instances. We were able to do this because the instance dimensions we have focused on, i.e., the dimensions that regularly appear on Spliddit, are rather small. In general, however, computing the valuation distance is NP-hard (Appendix B.1), and would be prohibitively slow to compute for, say, instances with dimensions $n = m = 10$ (even with an integer linear programming solver).

To verify that the patterns we described above extend to large (synthetic) instances, and to ready our mapping approach for a future in which larger fair-division problems might be routinely solved, we define in Appendix B.2 the *demand distance*, a heuristic approximation to the valuation distance. Crucially, the demand distance between two instances can be computed in polynomial time by finding a maximum-weight bipartite matching, which is also fast in practice. Though the demand distance may, in principle, deviate substantially from the valuation distance, we find that both correlate very well, with a Pearson correlation coefficient of at least 97% across our dimensions (Fig. 5 in Appendix B.1 correlation diagrams). Maps resulting from both distances are virtually indistinguishable, which is demonstrated by numerous juxtaposition figures in Appendix D.

Using this demand distance, we compute a distance-embedding map for $n = 10$ and $m = 20$, which we defer to Appendix D due to space limitations.⁷ The broad patterns we observed in 3×6 and 5×5 instances continue to hold, which we have also confirmed for even

⁶In Appendix D, we show that resampling instances continue to cover the embedding map for substantially larger instance dimensions ($n = 10, m = 20$), using the methodology of Section 3.3.

⁷Since none of the real-world instances are this large, and since i.i.d. and attributes instances are even more clustered around indifference, we focus on resampling instances. In Appendix A.2, we give details about the instances chosen, and show how the model's parameters determine the instances location on the map.

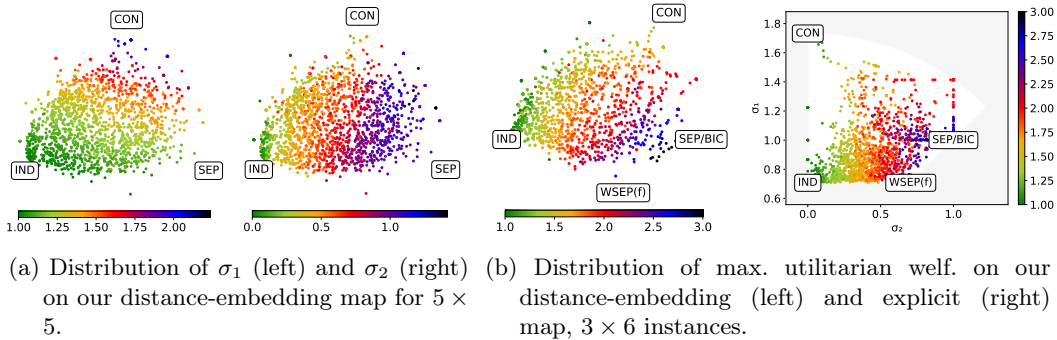


Figure 2: Distributions of the σ_1, σ_2 values and comparison of the two maps we introduce.

larger instances (Appendix A.3). Creating maps using the demand distance scales readily to larger sizes—even, say, to $n = m = 100$.

4 Explicit Maps

Generating maps through a distance embedding entails several inherent disadvantages:

Instability. The distance-embedding map may change non-continuously as the result of slight changes to the random seed or the set of mapped instances (though we did not observe this, Appendix A.1).

Data dependence. Suppose that you want to place an allocation instance on the map to predict its properties. This would require data for all other instances and computing pairwise distances, which would be more difficult than directly computing your instance’s properties.

Theoretical intractability. Which instances are “most extreme”? Where do instances from a probability distribution lie on the map? One can answer such questions empirically, but not theoretically.

To overcome these challenges, we propose an *explicit map* of fair division instances: a function μ from allocation instances to \mathbb{R}^2 , which replicates the general layout of the distance-embedding map. Specifically, this function maps $n \times m$ utility matrices as follows:

$$\mu : \mathbb{R}^{n \times m} \rightarrow \mathbb{R}^2 \quad U \mapsto (\sigma_1(U), \sigma_2(U)),$$

where $\sigma_1(U)$ and $\sigma_2(U)$ are the largest and second-largest singular values of the matrix U , respectively. As Fig. 2a shows (on the same 5×5 map as in Fig. 1), these two values closely capture the vertical and horizontal ordering of instances in our distance-embedding map, ensuring that the two maps are closely aligned (Fig. 8 in Appendix C shows the corresponding 3×6 map). In this section, we show that the explicit map is similarly informative as the distance-embedding map, while being stable, data independent, and theoretically tractable by design.

4.1 Demystifying the Singular Value Map

We begin by recalling facts about singular values that make them suitable components for our explicit map function. First, the singular values are invariant under permutations of rows or columns in the utility matrix, so that relabeling agents or goods will not change the map embedding. Second, σ_1 and σ_2 are 1-Lipschitz continuous in the entries of the matrix, which together with the previous point implies that two instances with small valuation distance must be placed near each other on the explicit map. Third, adding a column of zeros, i.e., a good that no agent values, does not change the singular values, which means that

instances can be naturally compared across different m . Finally, implementations of efficient algorithms for computing singular values are readily available (e.g., in numpy), which makes it easy to compute a given instance’s position on the map.

We now aim to give the reader an intuition for what information σ_1 and σ_2 express about an allocation instance and why. We begin with σ_1 , which can be expressed as

$$\sigma_1 = \max_{\vec{v}_1 \in \mathbb{R}^m, \|\vec{v}_1\|=1} \|U \vec{v}_1\|, \quad (1)$$

where $\|\cdot\|$ is the Euclidean (ℓ^2) norm. Since we rarely think about utility matrices as linear functions over unitary vectors, it is instructive to pretend that the norms in Eq. (1) were ℓ^1 -norms. In this case (choosing \vec{v}_1 nonnegative w.l.o.g.), the $U \vec{v}_1$ being optimized over are the convex combination of U ’s columns, for the coefficients given by \vec{v}_1 . If we were indeed maximizing the ℓ^1 -norm of $U \vec{v}_1$, σ_1 would be the largest column sum, or *maximum demand*. Though the ℓ^2 norm slightly complicates the picture,⁸ σ_1 and the maximum demand are very highly correlated: across our 3×6 instances, for example, the correlation coefficient is 97%. Thus, σ_1 can be understood as good approximation of the maximum demand, up to shifting and rescaling.

To interpret the second-largest singular value σ_2 , we recall how the singular value decomposition of an $\mathbb{R}^{n \times m}$ matrix U can be used to find a low-dimensional embedding of the row vectors (in our case, the agents’ utility vectors).⁹ For example, the line through the origin $span(\{\vec{v}_1\})$, spanned by the argmax of Eq. (1), is the best 1-dimensional space to embed the rows in, in the following sense: if we sum up, for each row $\vec{u}_i \in \mathbb{R}^m$, the squared length of its projection onto this space, $span(\{\vec{v}_1\})$ maximizes this sum across all 1-dimensional subspaces. In fact, this sum of squared projection lengths is σ_1^2 , which means that σ_1 measures “how much” of the row vectors can be captured by a 1-dimensional embedding. Similarly, σ_2 , which can be calculated as

$$\max_{\vec{v}_2 \in \mathbb{R}^m, \|\vec{v}_2\|=1, \vec{v}_2 \perp \vec{v}_1} \|U \vec{v}_2\|,$$

measures how much the row embedding improves when going from the optimal 1-dimensional space $span(\{\vec{v}_1\})$ to the optimal 2-dimensional space $span(\{\vec{v}_1, \vec{v}_2\})$.

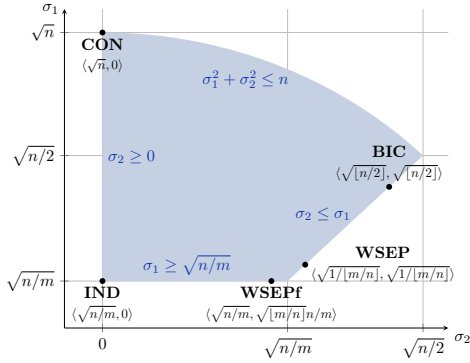
Thus, as a first approximation, σ_2 measures how diverse the agents’ utilities are. It is zero if all agents have the same utility vector, and large when there are blocks of agents that completely disagree on which goods have nonzero value. To again find a more elementary correlate, we define an instance’s *preference diversity* as the mean ℓ^2 distance between utility vectors, averaged over all pairs of agents in the instance. Again, we find a very high correlation (96% correlation coefficient for 3×6).

4.2 Theoretical Properties of the Map

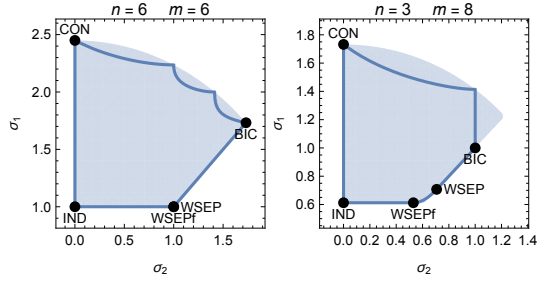
We now theoretically characterize the image of our map function μ for given dimensions n, m . Our task — characterizing the combinations of singular values in stochastic rectangular matrices — is of interest independently to our fair-division setting, but, to our knowledge, has not previously been undertaken. This process will give us a more precise understanding of what makes instances extreme along either dimension of our map. Figure 3a summarizes both the outlines of the map and the positions of characteristic instances, which can guide the reader through this section. We orient on the page such that σ_1 grows in the “North”

⁸It gives an advantage to combinations of columns in which several columns have positive coefficients, and it encourages making a few coordinates of $U \vec{v}_1$ large rather than all.

⁹See Chapter 3 by Blum et al. [2020] for a detailed explanation. Though singular values are closely connected to dimensionality reduction, our use is non-standard. Applying value decomposition directly to find a 2D embedding of utility matrices would result in embeddings highly sensitive to row and column permutations and would thus not be fruitful. One way to understand the discussion above is that we map each utility matrix to the square roots of the top-two eigenvalues in its principal component analysis; except that we do not shift column sums to zero, since this would, e.g., make IND and CON indistinguishable.



(a) Bounding inequalities of the map, and locations $\langle \sigma_1, \sigma_2 \rangle$ of characteristic instances.



(b) Explicit map for $\langle n, m \rangle = \langle 6, 6 \rangle$ and $\langle 3, 8 \rangle$. By Theorems 1 to 4, the map is contained in the shaded area. Lines trace interpolations between named instances (see Appendix C.1).

Figure 3: The general shape of the explicit map (left) and those for selected values of n and m (right).

and σ_2 in the “East” direction, which by Fig. 2a generally aligns with how we have presented the distance-embedding map.

Whereas CON and IND still mark the left corners of our map, the other two corners lead us to new characteristic instances. For the lower-right corner, we refine our definition of separability since SEP (with $\sigma_1 = \sigma_2 = 1$) only lies on the lower boundary if $n = m$. If m is a proper multiple of n , the lower-left corner is instead inhabited by *wide separability*, in which every agent values m/n disjoint goods, giving equal value n/m to each of them. In Appendix C.1.1, we extend wide separability to $n \nmid m$ in two slightly different ways: one, WSEP, always lies on the right border while the other, WSEPF always lies on the lower border.

The final characteristic instance is *bicontention* (BIC); here, half of the agents place all utility on one common good and half of the agents on a second common good (for odd n , one agent places all value on a third good). Since this instance combines highly demanded goods with sharply distinct utility vectors, it always lies on the right border and, for even n , is exactly located in the upper-right corner.

The main results of this section address all four sides of the map. For each side, we bound the map by an inequality and show that the inequality is sharp using our characteristic instances. For three of the sides, we give simple, necessary-and-sufficient conditions for an instance lying on the boundary. If n is even and divides m , as in the left subplot of Fig. 3b, our characteristic instances lie exactly in the four corner points of the map, and we can exactly trace three of the four sides by interpolating between corner instances. If these divisibility conditions do not hold, as illustrated in Fig. 3a and the right subplot of Fig. 3b, the characteristic instances lie in the corner up to rounding terms. Proofs of our characterizations tend to be short and cute, but are deferred to Appendix C.2.

Theorem 1 (“West”). σ_2 is at least 0. An instance lies on this boundary iff all agents have the same utility vector. In particular, IND, CON, and their convex combinations lie on this boundary.

Theorem 2 (“South”). σ_1 is at least $\sqrt{n/m}$. An instance lies on this boundary iff all columns of its utility matrix have an equal sum (namely, n/m). In particular, IND, WSEPF, and their convex combinations lie on this boundary.

Theorem 3 (“North”). σ_1 is at most $\sqrt{n - \sigma_2^2} \leq \sqrt{n}$. An instance lies on this boundary iff each agent values a single good, and if at most two goods are valued by any agent. In particular, CON and, if n is even, BIC lie on this boundary.

Theorem 4 (“East”). σ_2 is at most σ_1 . If U , after row and column permutation, has the block matrix structure $\begin{pmatrix} A & 0 & 0 \\ 0 & A & 0 \\ 0 & 0 & B \end{pmatrix}$ for rectangular matrices A, B and $\sigma_1(A) \geq \sigma_1(B)$, this is sufficient for lying on the boundary. (If B has height 0, we set $\sigma_1(B) = 0$.) In particular, WSEP, BIC, and a suitable interpolation lie on this boundary.

We conclude the theoretical discussion by pointing out that existing and future results in the theory of nonnegative random matrices have implications for our explicit map. For example, consider a random process in which a single utility vector is drawn from a flat Dirichlet distribution and duplicated for all agents (thus, $\sigma_2 = 0$). For this distribution over instances, Crumpton et al. [2022] recently derived that $\mathbb{E}[\sigma_1^2] = 2^{n/(n+1)}$ as well as formulas for σ_1^2 ’s higher moments. Brito et al. [2022] study a random process, in which, for fixed integers $d_2 \geq d_1 \geq 3$, an instance is uniformly chosen in which each agent values d_1 goods at value $1/d_1$, and each good is valued by d_2 agents. In this case, σ_1 is always $\sqrt{n/m}$, and the authors show that, as $m, n \rightarrow \infty$, σ_2 converges to $(\sqrt{d_1-1} + \sqrt{d_2-1})/d_1$ in probability.

4.3 Comparison of the Maps

Comparing the explicit map to our distance-embedding map (see, e.g., Fig. 2b for the largest achievable utilitarian welfare), we see that the two maps have a similar layout and communicate similar information overall. In Appendix D, we provide extensive diagrams showing that this similarity extends to other features, the identifiability of instance sources, and to the 5×5 instances as well.

One major difference is in how the density of instances varies across both maps. Whereas the distance-embedding map fills the map at a rather uniform density, which helps legibility, the explicit map clusters some instances very densely (e.g., near the South boundary and the $\sigma_2 = 1$ line in Fig. 2b). But these dense areas of the map seem to highlight meaningful clusters of similar instances, given that instance features tend to be homogeneous within these dense areas. The shape of instances in the explicit map can similarly highlight noteworthy patterns. For example, the straight lines at $\sigma_1 = \sqrt{2}$ and $\sigma_2 = 1$ in Fig. 2b are formed by instances in which several agents only value one good (see Fig. 18 in Appendix D). The distance-embedding map makes such phenomena much harder to spot.

Hence, and because of the advantages of stability, data independence, and theoretical tractability, we see the explicit map as broadly preferable over the distance-embedding map on our data. Nevertheless, the distance-embedding map plays a crucial role by justifying the explicit map: the relevance of the explicit map rests in large part on the fact that a general, previously established approach surfaced the two largest singular values as the most salient dimensions of difference between instances.

5 Conclusion

We hope that our exploration of allocation instances initiates discussions about which assumptions on such instances are supported by practice, and how fair-division theory can leverage these assumptions to provide algorithms with stronger fairness properties for the bulk of practical allocation instances.

The main limitation of our study is that—despite tapping into unconventional data sources—we were unable to test our approach on large, real-world allocation instances. This seems rooted in a broader limitation of the practice of fair division: large allocation problems are hardly ever solved, or the preference data are not made available. We believe that our community should strive to collect and share such datasets, as has been recently done for election data [Mattei and Walsh, 2013].

References

- G. Amanatidis, E. Markakis, A. Nikzad, and A. Saberi. Approximation algorithms for computing maximin share allocations. *ACM Transactions on Algorithms (TALG)*, 13(4): 1–28, 2017.
- G. Amanatidis, G. Birmpas, A. Filos-Ratsikas, A. Hollender, and A. A. Voudouris. Maximum Nash welfare and other stories about EFX. *Theoretical Computer Science*, 863:69–85, 2021.
- G. Amanatidis, H. Aziz, G. Birmpas, A. Filos-Ratsikas, B. Li, H. Moulin, A. A. Voudouris, and X. Wu. Fair Division of Indivisible Goods: Recent Progress and Open Questions. *Artificial Intelligence*, 322:103965, 2023.
- Anonymized. Personal communication, 2023.
- Y. Bai and P. Gözl. Envy-Free and Pareto-Optimal Allocations for Agents with Asymmetric Random Valuations. In *Proceedings of IJCAI-2022*, pages 53–59, 2022.
- Y. Bai, U. Feige, P. Gözl, and A. D. Procaccia. Fair Allocations for Smoothed Utilities. In *Proceedings of EC-22*, 2022.
- G. Benadè. Personal communication, 2023.
- G. Benadè, N. Itzhak, N. Shah, A. D. Procaccia, and Y. Gal. Efficiency and usability of participatory budgeting methods. unpublished, 2018.
- A. Blum, J. E. Hopcroft, and R. Kannan. *Foundations of Data Science*. Cambridge University Press, 2020.
- N. Boehmer, R. Bredereck, P. Faliszewski, R. Niedermeier, and S. Szufa. Putting a compass on the map of elections. In *Proceedings of IJCAI-2021*, pages 59–65, 2021.
- N. Boehmer, P. Faliszewski, R. Niedermeier, S. Szufa, and T. Wąs. Understanding distance measures among elections. In *Proceedings of IJCAI-2022*, pages 102–108, 2022.
- N. Boehmer, K. Heeger, and S. Szufa. A map of diverse synthetic stable roommates instances. In *Proceedings of AAMAS-23*, pages 1003–1011, 2023.
- R. Bredereck, A. Figiel, A. Kaczmarczyk, D. Knop, and R. Niedermeier. High-multiplicity fair allocation made more practical. In *Proceedings of AAMAS-21*, pages 260–268, 2021.
- G. Brito, I. Dumitriu, and K. D. Harris. Spectral gap in random bipartite biregular graphs and applications. *Combinatorics, Probability and Computing*, 31(2):229–267, 2022.
- E. Budish. The Combinatorial Assignment Problem: Approximate Competitive Equilibrium from Equal Incomes. *Journal of Political Economy*, 119(6):1061–1103, 2011.
- E. Budish, G. P. Cachon, J. Kessler, and A. Othman. Course match: A large-scale implementation of approximate competitive equilibrium from equal incomes for combinatorial allocation. *Operations Research*, 65(2):314–336, 2017.
- E. Budish, R. Gao, A. Othman, A. Rubinstein, and Q. Zhang. Practical algorithms and experimentally validated incentives for equilibrium-based fair division (A-CEEI). arXiv:2305.11406 [cs:GT], 2023.
- D. E. Campbell and J. S. Kelly. Impossibility theorems in the arrobian framework. In K. J. Arrow, A. K. Sen, and K. Suzumura, editors, *Handbook of Social Choice and Welfare*, volume 1, pages 35–94. Elsevier, 2002.

- I. Caragiannis, D. Kurokawa, H. Moulin, A. D. Procaccia, N. Shah, and J. Wang. The Unreasonable Fairness of Maximum Nash Welfare. *ACM Transactions on Economics and Computation*, 7(3):1–32, 2019.
- B. R. Chaudhury, J. Garg, and K. Mehlhorn. EFX exists for three agents. In *Proceedings of EC-20*, pages 1–19, 2020.
- M. J. Crumpton, Y. V. Fyodorov, and P. Vivo. Statistics of the largest eigenvalues and singular values of low-rank random matrices with non-negative entries, 2022.
- J. P. Dickerson, J. Goldman, J. Karp, A. D. Procaccia, and T. Sandholm. The computational rise and fall of fairness. In *Proceedings of AAAI-2014*, 2014.
- P. Faliszewski, A. Kaczmarczyk, K. Sornat, S. Szufa, and T. Waś. Diversity, agreement, and polarization in elections. In *Proceedings of IJCAI-2023*, pages 2684–2692, 2023.
- A. Farhadi, M. Ghodsi, M. T. Hajiaghayi, S. Lahaie, D. Pennock, M. Seddighin, S. Seddighin, and H. Yami. Fair allocation of indivisible goods to asymmetric agents. *Journal of Artificial Intelligence Research*, 64:1–20, 2019.
- J. Goldman and A. D. Procaccia. Spliddit: Unleashing fair division algorithms. *ACM SIGecom Exchanges*, 13(2):41–46, 2014.
- J. Kruskal. Multidimensional scaling by optimizing goodness of fit to a nonmetric hypothesis. *Psychometrika*, 29(1):1–27, 1964.
- D. Kurokawa, A. D. Procaccia, and J. Wang. When can the maximin share guarantee be guaranteed? In *Proceedings of AAAI-2016*, pages 523–529, 2016.
- R. J. Lipton, E. Markakis, E. Mossel, and A. Saberi. On approximately fair allocations of indivisible goods. In *Proceedings of EC-04*, pages 125–131, 2004.
- P. Manurangsi and W. Suksompong. When Do Envy-Free Allocations Exist? In *Proceedings of AAAI-2019*, pages 2109–2116, 2019.
- P. Manurangsi and W. Suksompong. Closing Gaps in Asymptotic Fair Division. *SIAM Journal on Discrete Mathematics*, 35(2):668–706, 2021.
- N. Mattei and T. Walsh. Preflib: A library for preferences. In *Proceedings of ADT-13*, pages 259–270, 2013.
- B. Plaut and T. Roughgarden. Almost Envy-Freeness with General Valuations. *SIAM Journal on Discrete Mathematics*, 34(2):1039–1068, 2020.
- T. Roughgarden. Distributional Analysis. In T. Roughgarden, editor, *Beyond the Worst-Case Analysis of Algorithms*, pages 167–188. Cambridge University Press, 2020.
- W. Shafer and H. Sonnenschein. Market demand and excess demand functions. In K. J. Arrow and M. D. Intriligator, editors, *Handbook of Mathematical Economics*, volume 2, pages 671–693. Elsevier, 1982.
- N. Shah. Personal communication, 2022.
- S. Szufa, P. Faliszewski, P. Skowron, A. Slinko, and N. Talmon. Drawing a map of elections in the space of statistical cultures. In *Proceedings of AAMAS-20*, pages 1341–1349, 2020.
- S. Szufa, P. Faliszewski, L. Janeczko, M. Lackner, A. Slinko, K. Sornat, and N. Talmon. How to sample approval elections? In *Proceedings of IJCAI-2022*, pages 496–502, 2022.

user1551 on Math Stack Exchange. Characterize stochastic matrices such that max singular value is less or equal one. Mathematics Stack Exchange, 2018. <https://math.stackexchange.com/q/1129977>, access: Jan 8, 2023.

H. R. Varian. Equity, envy, and efficiency. *Journal of Economic Theory*, 9(1):63–91, 1974.

APPENDIX

A Details on Datasets and Experiments

We combined various statistical cultures and the real-world data to construct datasets that we focus on in the paper. The real-world datasets are available upon request from the authors of the corresponding works cited in Section 2.2, from whom we also got permission to use the data in our study.

A.1 Datasets 5×5 and 3×6

For the 5×5 dataset consisting of instances with 5 agents and 5 goods, we generated 40 instances according to: the attributes models with 2 and 5 attributes; the resampling model with all values $\{0.2, 0.4, 0.6, 0.8\}$ of parameter p and all values $\{0.2, 0.8\}$ of parameter ϕ . Next, we generated 40 instances with i.i.d. valuations taking the uniform distribution over $[0, 1]$ and the same number of instances with i.i.d. valuations with the exponential distribution (recall that here the distribution’s rate does not change the outcome due to rescaling). Furthermore, we added 500 instances sampled (as described in the previous section) from the Island data, 500 instances from the Candies data, and all 16 Spliddit instances. Finally, we put the respective CON, IND, SEP, WSEP, and BIC instance. Analogously, we constructed the 3×6 dataset consisting of instances with 3 agents and 6 goods. The only exception being that in the 3×6 dataset, we took 250 instances each of the Island, Candies, and Spliddit data, which is possible since there were enough Spliddit instances of this size.

We generated each of the datasets multiple times (note that generating real-life inspired data is a random process) and repeated all our experiments. The obtained results were qualitatively the same.

A.2 Dataset 10×20

To verify that the instances coming from the resampling model cover diverse areas of our maps, we also constructed a dataset consisting of $n = 10$ agents and 20 goods. In this dataset, besides the CON, IND, and SEP instances, we generated 4 instances per each combination of parameters $p \in \{0.05, 0.1, 0.2, 0.4, 0.6, 0.8\}$ and $\phi \in \{0.05, 0.1, 0.25, 0.5, 0.75, 0.9, 0.95\}$. We did not include instances sampled from real-world distributions as none of them have more than 10 goods, and cloning them could change the structure of the instances in an unpredictable manner. As our goal was to cover the whole space, we also omitted the i.i.d. and attributes models since they tend to cluster in very specific and small areas of the map. Indeed, this behavior can already be observed for the 3×6 and 5×5 datasets in Figs. 21 to 23 in Appendix D. Note that numerous juxtapositions of our datasets in Appendix D present that the 10×20 dataset yields a similarly structured distribution of values of natural features across the map, as compared to our canonical 3×6 and 5×5 datasets. Since computing the valuation distance for instances in the 10×20 dataset is computationally too demanding, for this dataset we only computed maps using the demand distance.

In Fig. 4, we show how each value of p and ϕ traces a shifting band on the map, which enables the distribution to cover the entire distance-embedding map.

A.3 Larger Instances

Finally, to check scalability of the demand distance, we also conducted our experiments on data with larger numbers of goods and agents. We computed the maps for maximum instance sizes of $n = m = 300$ on a standard laptop computer¹⁰. For example, computing

¹⁰Specifically, we used two machines for the experiments we present: Apple® MacBook Pro® (Apple M2 Max, 64GB RAM) and HP® ProBook 650 G8 (11th Gen Intel® Core™ i5-1135G7 @ 2.40GHz, 32GB RAM). We computed the embeddings on the first one and the feature values on the second one. In the

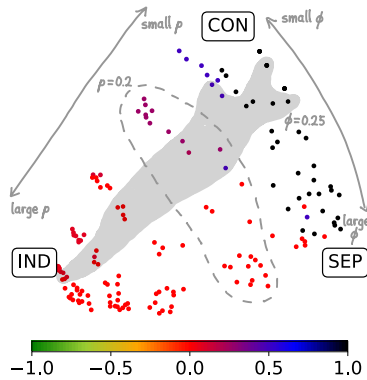


Figure 4: Distance-embedding map for the demand distance, containing 10×20 instances drawn from the resampling model. Colors indicate minimax envy. Hand-written annotations show placement of resampling instances for different p, ϕ .

the demand distance between a pair of them took, on average, $1/11$ seconds and 1.2 seconds for, respectively instance sizes $n = m = 100$ and $n = m = 300$. This gives, respectively, around 20 minutes and slightly above 3.5 hours to compute maps of the datasets analogous to the above-described 10×20 one. We emphasize that the running time of our algorithm for computing the demanding distance depends quadratically on the number of instances in the dataset and nonlinearly only on the *minimum* of n and m . Hence, the running times grow roughly linearly for larger instance sizes, as long as $\min(n, m) = 300$ (we verified it for instances with the number of either agents or goods being 1000, which increased the running time only at most twice). The given running times do not include computing the values of features — studying effective and scalable ways of computing them is not a goal of our study.

The results were qualitatively the same, so not to overload the paper with more pictures, we omit the computed maps.

B Deferred Details from Section 2

Valuation Distance

Consider a set $[n]$ of agents, a set $[m]$ of resources and some allocation instances $U \in \mathbb{R}_{\geq 0}^{n \times m}$ and $U' \in \mathbb{R}_{\geq 0}^{n \times m}$. Denote by Π_A and Π_m the sets of, respectively, all permutations $[n] \rightarrow [n]$ and $[m] \rightarrow [m]$. Then, consider some $\pi_a \in \Pi_A$ and some $\pi_{goods} \in \Pi_m$, which we call, respectively, an *agent matching* and a *good matching*. For some distance δ on nonnegative real numbers, we let

$$D_\delta(U, U', \pi_a, \pi_{goods}) := \sum_{i \in [n]} \sum_{j \in [m]} \delta(u_{i,j}, u_{\pi_a(i), \pi_{goods}(j)})$$

and refer to $D_\delta(U, U', \pi_a, \pi_{goods})$ as the δ -distance between U and U' *witnessed by* π_a and π_{goods} . The δ -distance between U and U' , denoted by $d_\delta(U, U')$, is then the minimal δ -distance between U and U' witnessed over all pair of matchings; formally:

$$d_\delta(U, U') := \min_{\pi'_a \in \Pi_A, \pi'_{goods} \in \Pi_m} D_\delta(U, U', \pi'_a, \pi'_{goods}).$$

course of the full research project we also used an Ubuntu 22.04.4 LTS server (Intel[®] Xeon[®] Silver 4310 CPU @ 2.10GHz with 12 physical cores, 128GB RAM). We, however, do not present any results obtained using this machine.

We are now ready to formally define our *valuation distance* that, intuitively, is the smallest sum of difference in agents valuations of the goods achievable over all possible matchings of agents and goods.

Definition 1. Given two allocation instances $U \in \mathbb{R}_{\geq 0}^{n \times m}$ and $U' \in \mathbb{R}_{\geq 0}^{n \times m}$ with n agents and m goods, its *valuation distance* $d_v(U, U')$ is:

$$d_v(U, U') := d_{\ell_1}(U, U') := \min_{\pi_a, \pi_{goods}} \sum_{i \in [n]} \sum_{j \in [m]} \left| u_{i,j} - u'_{\pi_a(i), \pi_{goods}(j)} \right|.$$

It is easy to see that that the valuation distance is isomorphic. Naturally, if the tasks are isomorphic, then there exists some pair of agent and good matchings that witness distance 0. On the other hand, if there is no such pair, there is no possibility that the valuation distance is 0. The property of being an isomorphic distance, however, comes at a cost of computational intractability.

B.1 Valuation Distance Hardness

Theorem 5. Given two task allocations $U \in \mathbb{R}_{\geq 0}^{n \times m}$ and $U' \in \mathbb{R}_{\geq 0}^{n \times m}$ and an real number d , deciding whether $d_v(U, U') \leq d$ is NP-hard.

Proof. We give a polynomial-time many-one reduction from an NP-hard problem $d_{\text{Spear-Isomorphic Distance}}$. In this problem we are given two ordinal elections $E = (C, V)$ and $E' = (C', V')$ such that $|C| = |C'|$ and $|V| = |V'|$ and an integer k . Assuming that for some voter a and candidate b , where both a and b are part of the same election E , we denote by $\text{pos}_a^E(b)$ the position of candidate b according to the ranking of a , we ask whether there exist two permutations $\rho: C \rightarrow C'$ and $\phi: V \rightarrow V'$ such that

$$D(\rho, \phi) := \sum_{v \in V} \sum_{c \in C} \left| \text{pos}_v^E(c) - \text{pos}_{\phi(v)}^{E'}(\rho(c)) \right| \leq k.$$

Given the instance I of $d_{\text{Spear-Isomorphic Distance}}$ as described above, our reduction constructs an instance I' of our problem as follows. We first construct allocation instance U using election E from the original instance. Allocation instance U consists of $n := |V|$ agents $[n]$ representing voters and $m := |C|$ goods $[m]$. Thus, U is a matrix of dimension $n \times m$. Taking a normalizing factor $F = 1 + 2 + \dots + |C| = \binom{|C|}{2}$, for each voter $v_i \in V$ and candidate $c_j \in C$, we set the corresponding agent i 's utility for good j to be $u_{i,j} = \text{pos}_{v_i}^E(c_j)/F$. It can be easily verified that the values of the utility function of each agent in U (that is, the values of each row of U) sum to 1. We obtain instance I' , by analogously constructing allocation instance U' using election E' and setting the distance d in question (regarding instance I') to $d := k/F$.

We show that for each pair of permutations $\rho: C \rightarrow C'$ and $\phi: V \rightarrow V'$ such that $D(\rho, \phi) \leq k$, there are two permutations π_a and π_{goods} such that witness that $d_v(U, U') \leq d$. Since we also show that the opposite direction is true, we obtain the reduction's correctness.

Suppose that we have ρ and ϕ that meet the above assumption. Consider the following π_a and π_{goods} . For each voter $v_i \in V$ and candidate $c_j \in C$, let $\pi_a(i) = i'$ such that $\phi(v_i) = v_{i'}$, and $\pi_{goods}(j) = j'$ such that $\phi(c_j) = c_{j'}$. In words, permutation π_a maps agents exactly as permutation ϕ maps their respective voters, and so does permutation π_{goods} with respect to goods and candidates. Now, in the series of algebraic transformations, let us analyze the

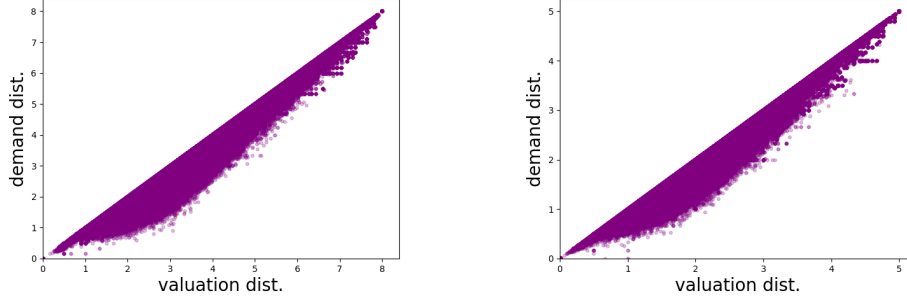


Figure 5: Correlation between our distances for the 5×5 dataset (left) and the 3×6 dataset (right).

relation of $D(\rho, \phi)$ and d :

$$\begin{aligned}
 D(\rho, \phi)/F &= \frac{\sum_{v_i \in V} \sum_{c_j \in C} \left| \text{pos}_{v_i}^{E'}(c_j) - \text{pos}_{\phi(v_i)}^{E'}(\rho(c_j)) \right|}{F} = \\
 &= \sum_{v_i \in V} \sum_{c_j \in C} \left| \frac{\text{pos}_{v_i}^{E'}(c_j)}{F} - \frac{\text{pos}_{\phi(v_i)}^{E'}(\rho(c_j))}{F} \right| = \\
 &= \sum_{v_i \in V} \sum_{c_j \in C} \left| u_{i,j} - u'_{\pi_a(i), \pi_{goods}(j)} \right| = \\
 &= \sum_{i \in [n]} \sum_{j \in [m]} \left| u_{i,j} - u'_{\pi_a(i), \pi_{goods}(j)} \right| = d.
 \end{aligned}$$

So, clearly, if $D(\rho, \phi) \leq k$, then $d_v(U, U')$ witnessed by π_a and π_{goods} is smaller than $k/F = d$. On the other hand, if there exist π_a and π_{goods} that witness $d_v(U, U') \leq d$, then one can construct ρ and ϕ for which $D(\rho, \phi) \leq dF = k$. \square

The computational hardness of the task of computing the valuation distance comes from the fact that one seeks an optimal value depending on two matchings simultaneously. It turns out that this intuitive understanding can be well supported by a formal claim. We show that for a given either the agent matching or the good matching, the optimal value of the distance as witnessed by the given matching can be computed in polynomial-time.

Theorem 6. *Given two allocation instances U, U' , a (fixed) agent matching π_a , a real number d , deciding whether $d_v(U, U')$ as witnessed by π_a is at most d is polynomial-time solvable. The same holds for the case of a given good matching.*

Proof. Let us fix numbers n and m of, respectively, agents and goods. For two allocation instances $U \in \mathbb{R}_{\geq 0}^{n \times m}$ and $U' \in \mathbb{R}_{\geq 0}^{n \times m}$ and an agent matching $\pi_a: [n] \rightarrow [n]$, we give a polynomial-time algorithm that computes a good matching $\pi_{goods}: [m] \rightarrow [m]$ minimizing

$$D(\pi_{goods}) := \sum_{i \in [n]} \sum_{j \in [m]} \left| u_{i,j} - u_{\pi_a(i), \pi_{goods}(j)} \right|.$$

In words, the algorithm computes the minimal achievable distance as witnessed by the given agent matching π_a .

The algorithm constructs a complete bipartite weighted graph G consisting of vertices x_1, x_2, \dots, x_m of one partition and consisting of vertices y_1, y_2, \dots, y_m of the other partition. For each pair $i \in [n], j \in [m]$, the weight $w(\{x_i, y_j\})$ of edge $\{x_i, x_j\}$ is equal

$$\text{IND}_m := \begin{bmatrix} 1/m & 1/m & \cdots & 1/m \\ 1/m & 1/m & \cdots & 1/m \\ \vdots & \vdots & \ddots & \vdots \\ 1/m & 1/m & \cdots & 1/m \end{bmatrix} \quad \text{SEP}_m := \begin{bmatrix} 1 & 0 & \cdots & 0 \\ 0 & 1 & \cdots & 0 \\ \vdots & \vdots & \ddots & \vdots \\ 0 & 0 & \cdots & 1 \end{bmatrix} \quad \text{CON}_m := \begin{bmatrix} 1 & 0 & \cdots & 0 \\ 1 & 0 & \cdots & 0 \\ \vdots & \vdots & \ddots & \vdots \\ 1 & 0 & \cdots & 0 \end{bmatrix}$$

Figure 6: Matrices representing characteristic instances: Indifference (IND), Separability (SEP), and Contention (CON).

to $\sum_{\ell \in [n]} |u_{\ell,i} - u_{\pi_a(\ell),j}|$. Finally, the algorithm looks for a minimum weight perfect matching (which always exists) in G .

Let M be some perfect matching in G . Clearly, this perfect matching corresponds to exactly one good matching $\pi'_{goods}: [n] \rightarrow [n]$. Let us now compute the weight $w(M)$ of M :

$$\begin{aligned} w(M) &= \sum_{\{x_i, y_j\} \in M} \sum_{\ell \in [n]} |u_{\ell,i} - u_{\pi_a(\ell),j}| = \\ &= \sum_{\ell \in [n]} \sum_{\ell' \in [m]} |u_{\ell,\ell'} - u_{\pi_a(\ell),\pi'_{goods}(\ell')}| = D(\pi'_{goods}). \end{aligned}$$

Since our algorithm finds the minimum-weight matching, the correctness follows.

The algorithm runs in polynomial time because finding a minimum-weight matching is well-known polynomial-time solvable task and building the bipartite graph is quadratic with respect to the number of goods (which is polynomially bounded in the input size). The proof for the case of a given good matching is analogous. \square

B.2 Demand Distance and Distances Properties

In this section, we formally introduce the *demand distance* and we show the properties of both the demand and the valuation distances.

Demand Distances

Here, for each good of both instances, we build a *demand vector* containing the utility values that the good receives from different agents, sorted in decreasing order. We then find a mapping of vectors from one instance to the other that minimizes the sum of ℓ_1 distances of the mapped pairs. Hence, we obtain the following formal definition.

Definition 2. Let U^1 and U^2 be two allocation instances with n agents and m goods. The *demand vector* $\overrightarrow{\text{dem}}_U(j)$ of good $j \in [m]$ of instance U is the vector $(u_{1,j}, u_{2,j}, \dots, u_{n,j})$ sorted in descending order. Denoting by Π_{goods} all permutations of $[m]$, the *demand distance* $d_v(U^1, U^2)$ of U^1 and U^2 is

$$\min_{\pi_{goods} \in \Pi_{goods}} \sum_{j \in [m]} \|\overrightarrow{\text{dem}}_{U^1}(j) - \overrightarrow{\text{dem}}_{U^2}(\pi_{goods}(j))\|_1.$$

Due to the fact that this definition optimizes over only a single permutation, the demand distance can be computed in polynomial-time by finding a minimum matching in a weighted bipartite graph representing the contributions to the distance from matchings between each pair of agents.

Theorem 7. *Given two task allocations U and U' and a real number d , deciding whether it holds that $d_d(U, U') \leq d$ is polynomial-time solvable.*

Proof. We give an algorithm that first constructs a weighted bipartite graph (representing the task of computing the demand distance) and then computes its minimum weight perfect matching, which represents the optimal good matching.

To be specific, our algorithm proceeds as follows. For each $r \in \mathcal{R} \cup \mathcal{R}'$, it first computes $\overrightarrow{\text{dem}}(r)$. Then, it constructs a bipartite graph G with one partition consisting of the goods \mathcal{R} and the other one of the goods \mathcal{R}' . For every pair $(r, r') \in \mathcal{R} \times \mathcal{R}'$, the algorithm adds an edge $\{r, r'\}$ to G and sets its weight $w(r, r') := d_{\ell_1}(\overrightarrow{\text{dem}}(r), \overrightarrow{\text{dem}}(r'))$. Finally, the algorithm finds a minimum weight perfect matching, say M , of G .

Since M is a perfect matching (and $|\mathcal{R}| = |\mathcal{R}'|$), it is clear that M represents a good matching π_{goods} such that for each $\{r, r'\} \in M$, $\pi_{\text{goods}}(r) = \pi_{\text{goods}}(r')$. Hence, the total weight $w(M)$ of M can be expressed as

$$w(M) := \sum_{\{r, r'\} \in M} d_{\ell_1}(\overrightarrow{\text{dem}}(r), \overrightarrow{\text{dem}}(r')) = \sum_{r \in \mathcal{R}} d_{\ell_1}(\overrightarrow{\text{dem}}(r), \overrightarrow{\text{dem}}(\pi_{\text{goods}}(r))).$$

As a result, a minimum weight perfect matching in graph G yields a good matching that witnesses the demand distance and the weight of this matching is exactly the requested demand distance.

Computing a minimum weight perfect matching is polynomial-time solvable. Thus, our algorithm also runs in polynomial time. \square

Note that the procedure described in the proof of Theorem 7 is constructive and, in fact, solves the optimization variant of the problem of computing the demand distance between two allocation tasks.

The improvement in the running time of computing the demand distance in comparison to that of the valuation distance comes at a cost. The demand distance ignores information about the identity of agents, which can lead two non-isomorphic instances to be at distance 0 from each other (see Fig. 7).

Maximal Values of Valuation and Demand Distances

We show the upper-bound on the values of both distances in the following technical proposition.

Proposition 1. *Let U and U' be two allocations instances with n agents and m goods. Then, the valuation distance $d_v(U, U')$ and the demand distance $d_d(U, U')$ are at most $2n - \frac{2n}{m}$.*

For the proof of this proposition, we will first require the following lemma:

Lemma 1 (Rearrangement Inequality). *Let \vec{x} and \vec{y} be two size n vectors whose entries are sorted non-increasingly. Then, for every permutation σ of $[n]$, it holds that*

$$\sum_{i \in [n]} \min(x_i, y_i) \geq \sum_{i \in [n]} \min(x_i, y_{\sigma(i)}).$$

Proof. The proof works recursively as follows: Assume that the smallest entry of \vec{y} would not be in the last position n , but in the position i^* . Consider two cases.

First, $x_n \leq y_{i^*}$. Since by definition $y_n \geq y_{i^*}$, swapping y_{i^*} and y_n cannot decrease the overall sum.

Second, $x_n > y_{i^*}$. Then, also $x_{i^*} > y_{i^*}$ (by \vec{x} being non-increasing). That is, swapping y_{i^*} and y_n leads the minimum in position n to become y_{i^*} (the previous minimum of position i^*). Yet, the minimum in position i^* is now at least $\min(y_n, x_{i^*})$, which must be at least $\min(y_{i^*}, x_n)$, since $y_n \geq y_{i^*}$ and $x_{i^*} \geq x_n$.

The last position is correct, that is, remove these entries and recurse. \square

Proof of Proposition 1. We first show the proof for the valuation distance. It is an adaption of the proof of Lemma 2 in the full version (arXiv:2205.00492 [cs.GT]) of Boehmer et al. [2022].

Assume towards a contradiction that we have two allocations instances U and U' with $d_v(U, U') > 2n - \frac{2n}{m}$. Assume w.l.o.g. that $d_v(U, U') = \sum_{i \in [n], j \in [m]} |u_{i,j} - u'_{i,j}|$. otherwise we could permute rows and column (relabel the goods and agents) of one of the allocation instances.

Observe that

$$\begin{aligned}
d_v(U, U') &= \sum_{i \in [n], j \in [m]} |u_{i,j} - u'_{i,j}| \\
&= \sum_{i \in [n], j \in [m]} (\max(u_{i,j}, u'_{i,j}) - \min(u_{i,j}, u'_{i,j})) \\
&= \sum_{i \in [n], j \in [m]} (u_{i,j} + u'_{i,j}) - 2 \sum_{i \in [n], j \in [m]} \min(u_{i,j}, u'_{i,j}) \\
&= \sum_{i \in [n]} 2 - 2 \sum_{i \in [n], j \in [m]} \min(u_{i,j}, u'_{i,j}) \\
&= 2n - 2 \sum_{i \in [n], j \in [m]} \min(u_{i,j}, u'_{i,j}). \tag{2}
\end{aligned}$$

If $d_v(U, U') > 2n - \frac{2n}{m}$, then it must hold that:

$$\sum_{i \in [n], j \in [m]} \min(u_{i,j}, u'_{i,j}) < n/m. \tag{3}$$

For each permutation σ of $[m]$, we have $d_v(U, U') \leq \sum_{i \in [n], j \in [m]} |u_{i,j} - u'_{i,\sigma(j)}|$ (this being incorrect would violate our assumption that $d_v(U, U') = \sum_{i \in [n], j \in [m]} |u_{i,j} - u'_{i,j}|$). Consequently, for every permutation σ of $[m]$, and reasoning analogously to Eq. (2) and Eq. (3), we get

$$\sum_{i \in [n], j \in [m]} \min(u_{i,j}, u'_{i,\sigma(j)}) < n/m.$$

Observe that if $x, y \in [0, 1]$, then it holds that $x \cdot y \leq \min(x, y)$. Since for each $i \in [n]$ and $j \in [m]$, we have $u_{i,j}, u'_{i,j} \in [0, 1]$, for each each permutation σ of $[m]$, it holds that:

$$\sum_{i \in [n], j \in [m]} u_{i,j} \cdot u'_{i,\sigma(j)} < n/m. \tag{4}$$

We define a family $\Psi := \{\sigma^{(k)} \mid k \in [m]\}$ of permutations using functions $\sigma^{(k)}(j) := (j + k - 1 \bmod m) + 1$. By summing up Eq. (4) (on both sides) for each permutation from Ψ we obtain:

$$\sum_{\sigma \in \Psi} \sum_{i \in [n], j \in [m]} u_{i,j} \cdot u'_{i,\sigma(j)} < n/m \cdot |\Psi|,$$

which can be rearranged to

$$\sum_{i \in [n], j \in [m]} u_{i,j} \cdot \sum_{\sigma \in \Psi} (u'_{i,\sigma(j)}) < n/m \cdot |\Psi|. \tag{5}$$

Since $\sum_{j \in [m]} u_{i,j} = \sum_{j \in [m]} u'_{i,j} = 1, \forall i \in [n]$, it holds that:

$$\sum_{\sigma \in \Psi} (u'_{i,\sigma(j)}) = \sum_{k \in [m]} (u'_{i,\sigma^{(k)}(j)}) = \sum_{\ell \in [m]} u'_{i,\ell} = 1.$$

allocation instance U	allocation instance U'		
u_1	2 4 6 8	u'_1	2 4 6 8
u_2	3 3 6 8	u'_2	3 3 6 8
u_3	6 8 6 0	u'_3	6 8 0 6
u_4	8 6 0 6	u'_4	8 6 6 0
Demand vectors of U		Demand vectors of U'	
	8 8 6 8		8 8 6 8
	6 6 6 8		6 6 6 8
	3 4 6 6		3 4 6 6
	2 3 0 0		2 3 0 0

Figure 7: Allocation instances demonstrating a zero demand distance (note the demand vectors and apply the identity matching) but a non-negative valuation distance (verify via an exhaustive check).

Hence (and with $|\Psi| = m$), from Eq. (5) we get

$$\sum_{i \in [n], j \in [m]} u_{i,j} < n,$$

which contradicts the fact that $\sum_{j \in [m]} u_{i,j} = \sum_{j \in [m]} u'_{i,j} = 1, \forall i \in [n]$. Hence, we have $d_v(U, U') \leq 2n - \frac{2n}{m}$.

To see that also $d_d(U, U') \leq 2n - \frac{2n}{m}$, we upper-bound $d_d(U, U') \leq d_v(U, U')$.

Assume towards a contradiction that the demand distance between two instances would be greater than the valuation distance. Let matrices $V = \overrightarrow{\text{dem}_U(1)} \cdots \overrightarrow{\text{dem}_U(m)}$ and $V' = \overrightarrow{\text{dem}_{U'}(\sigma(1))} \cdots \overrightarrow{\text{dem}_{U'}(\sigma(m))}$ be the matrices resulting from the column-wise concatenation of the demand vectors of U and U' , respectively, using some permutation σ of the columns.

Recall Eq. (2). Since the demand distance is upper-bounded by the entry-wise sum of ℓ^1 -distances between V and V' , the same reasoning as above holds. Thus,

$$\sum_{i \in [n], j \in [m]} \min(v_{i,j}, v'_{i,j}) < \sum_{i \in [n], j \in [m]} \min(u_{i,j}, u'_{i,j}), \quad (6)$$

Note that, Eq. 6 holds for any column permutation used to define V' , so in particular also when we use the same which we used for the valuation distance. In other words, we can assume that, up to permutation of the entries, U and V as well as U' and V' have the same column vectors.

For Eq. 6 to hold, it would need to hold that

$$\sum_{i \in [n]} \min(v_{i,j^*}, v'_{i,j^*}) < \sum_{i \in [n]} \min(u_{i,j^*}, u'_{i,j^*}) \quad (7)$$

for some column $j^* \in m$. Due to the rearrangement inequality (Lemma 1), however, we know that $\sum_{i \in [n]} \min(v_{i,j^*}, v'_{i,j^*}) \geq \sum_{i \in [n]} \min(u_{i,j^*}, u'_{i,j^*})$; a contradiction to Eq.7. \square

C Deferred Details from Section 4

An analogous map to the map presented in Fig. 2a can be seen in Figure 8, in which the distribution of σ_1 and σ_2 on our distance-embedding map is shown for the 3×6 instances.

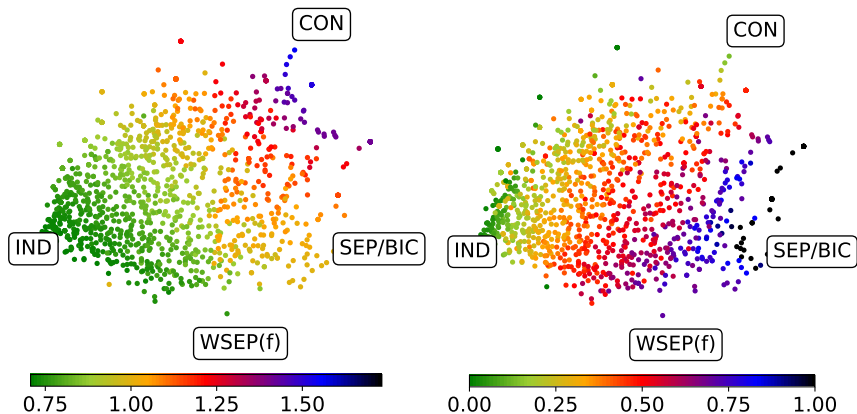


Figure 8: Distributions of the σ_1 (left) and σ_2 (right) values on our distance-embedding map using the valuation distance for the 3×6 instances.

C.1 Deferred Details from Section 4.2

C.1.1 Wide Separability

We propose two ways of generalizing this instance to m not divisible by n , setting $\ell := \lfloor m/n \rfloor$: In the first variant, WSEP, each agent values ℓ goods at $1/\ell$, and thus $m \bmod n$ goods have no value for any agent. In the second variant, WSEPF, each agent values the ℓ goods that no other agent values at n/m , and the final $m \bmod n$ goods have a value of $\frac{1-\ell n/m}{m \bmod n}$ for every agent. WSEP always lies on the East and WSEPF on the South border; if $n \mid m$, they coincide, meeting in the South-East corner.

C.2 Deferred Proofs

Theorem 1 (“West”). σ_2 is at least 0. An instance lies on this boundary iff all agents have the same utility vector. In particular, IND, CON, and their convex combinations lie on this boundary.

Proof. Singular values are always nonnegative real numbers. It is well-known that the second singular value is 0 if and only if the matrix has rank 1 (or zero), i.e., if all rows are linearly dependent. Since all row sums are 1, this is equivalent to all rows being identical. Since IND and CON each have only identical rows, they have $\sigma_2 = 0$. The same property is inherited by their convex combinations, which, by the continuity of the singular values, must trace the entire boundary between IND and CON. \square

Theorem 2 (“South”). σ_1 is at least $\sqrt{n/m}$. An instance lies on this boundary iff all columns of its utility matrix have an equal sum (namely, n/m). In particular, IND, WSEPF, and their convex combinations lie on this boundary.

Proof. By Eq. (1),

$$\begin{aligned}
\sigma_1 &= \max_{\vec{v}_1 \in \mathbb{R}^m, \|\vec{v}_1\|=1} \|U \vec{v}_1\| \\
&\geq \left\| U \begin{pmatrix} 1/\sqrt{m} \\ 1/\sqrt{m} \\ \vdots \\ 1/\sqrt{m} \end{pmatrix} \right\| \\
&= \left\| \begin{pmatrix} 1/\sqrt{m} \\ 1/\sqrt{m} \\ \vdots \\ 1/\sqrt{m} \end{pmatrix} \right\| && \text{(by row stochasticity)} \\
&= \sqrt{n/m}.
\end{aligned}$$

Note that the vector being multiplied with U in the second row has dimension m (thus norm 1), but the vector in the third row has dimension n .

We now show that, whenever this inequality is tight, all column sums must be n/m . This extends a widely known proof (presentation adapted from user1551 on Math Stack Exchange [2018]) showing that, among square matrices, a row-stochastic matrix has $\sigma_1 = 1$ if and only if it is doubly stochastic, i.e., its column sums are also equal to one. In the following, we set $\mathbf{1}_t$ to denote the vector $\begin{pmatrix} 1 \\ \vdots \\ 1 \end{pmatrix} \in \mathbb{R}^t$, and denote the vector dot product by $\langle \cdot, \cdot \rangle$.

$$\begin{aligned}
m &= \frac{m}{n} \langle \mathbf{1}_n, \mathbf{1}_n \rangle \\
&= \frac{m}{n} \langle \mathbf{1}_n, U \mathbf{e}_m \rangle && \text{(by row stochasticity)} \\
&= \left\langle U^T \left(\frac{m}{n} \mathbf{1}_n \right), \mathbf{1}_m \right\rangle \\
&\leq \left\| U^T \left(\frac{m}{n} \mathbf{1}_n \right) \right\| \cdot \|\mathbf{1}_m\| && \text{(Cauchy-Schwartz)} \\
&\leq \sigma_1(U^T) \frac{m}{n} \|\mathbf{1}_n\| \|\mathbf{1}_m\| && \text{(property of Operator Norm)} \\
&= \sigma_1(U) \frac{m}{n} \|\mathbf{1}_n\| \|\mathbf{1}_m\| && (\sigma_1(A) = \sigma_1(A^T)) \\
&= \sqrt{\frac{n}{m}} \frac{m}{n} \|\mathbf{1}_n\| \|\mathbf{1}_m\| && \text{(by assumption)} \\
&= \sqrt{\frac{n}{m}} \frac{m}{n} \sqrt{n} \sqrt{m} \\
&= m.
\end{aligned}$$

Since both ends of the inequality chain are equal, all terms along the chain must be equal. Since the Cauchy-Schwartz step was an equality, we know that $U^T (m/n \mathbf{1}_n)$ is a scalar multiple of $\mathbf{1}_m$; since $\|U^T (m/n \mathbf{1}_n)\| \|\mathbf{1}_m\| = m$, we now that $\|U^T (m/n \mathbf{1}_n)\| = \sqrt{m}$; finally, we now that $U^T (m/n \mathbf{1}_n)$ is nonnegative. Taking these facts together, we conclude that $U^T (m/n \mathbf{1}_n) = \mathbf{1}_m$, which means that all column sums of U are equal to n/m .

It is easy to see that IND, WSEPF, and their linear interpolations all have column sums of n/m , which concludes the claim. \square

Theorem 3 (“North”). σ_1 is at most $\sqrt{n - \sigma_2^2} \leq \sqrt{n}$. An instance lies on this boundary iff each agent values a single good, and if at most two goods are valued by any agent. In particular, CON and, if n is even, BIC lie on this boundary.

Proof. Setting $\sigma_1, \sigma_2, \dots, \sigma_r$ for the singular values of some matrix, it is well known that $\sum_{t=1}^r \sigma_t^2$ equals the square of the matrix’ Frobenius norm, i.e., equals the sum of squares

across the entries of the matrix. That is, for a matrix U ,

$$\sum_{t=1}^r \sigma_t^2 = \sum_{i=1}^n \sum_{j=1}^m u_{i,j}^2.$$

Since all entries of our matrix are between 0 and 1, the i th row's contribution to the right-hand side is $\sum_{j=1}^m u_{i,j}^2 \leq \sum_{j=1}^m u_{i,j} = 1$, and this inequality is tight if and only if agent i values one item at 1 and all others at 0. It follows that

$$\sigma_1^2 + \sigma_2^2 \leq \sum_{t=1}^r \sigma_t^2 \leq n,$$

where the inequality is tight exactly if and only if (a) all agents single-mindedly value a single good (which makes the second inequality tight) and (b) all σ_t for $t \geq 3$ are zero. Part (b) is the case if and only if U has rank at most 2. Assuming part (a), U 's rank is exactly the number of distinct goods which some agent values single-mindedly. Taking square, we obtain the desired inequality with its necessary-and-sufficient condition.

Clearly, this condition is satisfied by IND and by BIC if n is even. Note that there is a natural way to interpolate between these two, where one good is single-mindedly valued by t agents and a second good by $n - t$ agents. Clearly, each of these points lies on the boundary. If one linearly interpolates between successive values of t , the interpolations have one agent who values two items, which removes this interpolation point from the boundary. But of course this operation does not move the instance far from the boundary. Figure 3b shows this interpolation as the blue line following the upper boundary of the map. \square

Theorem 4 (“East”). σ_2 is at most σ_1 . If U , after row and column permutation, has the block matrix structure $\begin{pmatrix} A & 0 & 0 \\ 0 & A & 0 \\ 0 & 0 & B \end{pmatrix}$ for rectangular matrices A, B and $\sigma_1(A) \geq \sigma_1(B)$, this is sufficient for lying on the boundary. (If B has height 0, we set $\sigma_1(B) = 0$.) In particular, WSEP, BIC, and a suitable interpolation lie on this boundary.

Proof. $\sigma_2 \leq \sigma_1$ holds by definition of the singular values.

Let U be a utility matrix with the block matrix structure from the theorem statement (since the singular values are invariant to row and column permutations, it suffices to consider such matrices directly). One important property of singular values we have not used yet is that the singular values of a matrix U are the square roots of the eigenvalues of the Gram matrix $U^T U$ (or, equivalently, for $U U^T$).

Given the block matrix structure,

$$\begin{pmatrix} A & 0 & 0 \\ 0 & A & 0 \\ 0 & 0 & B \end{pmatrix} \begin{pmatrix} A & 0 & 0 \\ 0 & A & 0 \\ 0 & 0 & B \end{pmatrix}^T = \begin{pmatrix} AA^T & 0 & 0 \\ 0 & AA^T & 0 \\ 0 & 0 & BB^T \end{pmatrix}.$$

It is well known that the eigenvalues of such a block diagonal matrix are simply the eigenvalues of the blocks AA^T , AA^T , and BB^T combined (with multiplicity preserved), which means that the singular values of U are just the singular values of A , A , and B combined. In particular, all singular values of A will appear in U at least twice. By $\sigma_1(A) \geq \sigma_1(B)$, the largest singular value is one of these duplicated singular values, which implies that $\sigma_1(U) = \sigma_2(U) = \sigma_1(A)$.

After reshuffling the columns, WSEP looks as follows (setting again $\ell := \lfloor m/n \rfloor$):

$$\left(\begin{array}{ccc|ccc|cccccc} 1/\ell & \cdots & 1/\ell & 0 & 0 & 0 & 0 & 0 & 0 & 0 & 0 & 0 \\ 0 & 0 & 0 & 1/\ell & \cdots & 1/\ell & 0 & 0 & 0 & 0 & 0 & 0 \\ \hline 0 & 0 & 0 & 0 & 0 & 0 & 1/\ell & \cdots & 1/\ell & 0 & 0 & \cdots & 0 \\ & & & & & & & & & & & \ddots & \\ 0 & 0 & 0 & 0 & 0 & 0 & 0 & 0 & 0 & 0 & 1/\ell & \cdots & 1/\ell \end{array} \right)$$

where the lines indicate the division of the blocks. The symmetry of the instance ensures that (unless B has height 0) $\sigma_1(B) = \sigma_1(A)$, so WSEP lies on this boundary.

For BIC, the situation is even simpler:

$$\left(\begin{array}{c|c|ccc} 1 & 0 & 0 & 0 & \cdots & 0 \\ \vdots & 0 & 0 & 0 & \cdots & 0 \\ 1 & 0 & 0 & 0 & \cdots & 0 \\ \hline 0 & 1 & 0 & 0 & \cdots & 0 \\ \vdots & \vdots & 0 & 0 & \cdots & 0 \\ 0 & 1 & 0 & 0 & \cdots & 0 \\ \hline 0 & 0 & 1 & 0 & \cdots & 0 \end{array} \right)$$

In this case, the singular values are easy to calculate: $\sigma_1(A) = \sqrt{\lfloor n/2 \rfloor}$ which is at least $\sigma_1(B) = 1$.

Interpolating between both matrices without leaving the boundary is not straightforward. For this, we first linearly interpolate from WSEP to SEP. For some $0 < \theta < 1$, this means that each agent approves one good at $\theta + (1 - \theta)/\ell$ and $\ell - 1$ goods at $(1 - \theta)/\ell$. For this interpolation, the block structure remains the same as the one discussed for WSEP and preserves the same symmetry, which is why the interpolation stays on the boundary.

The interpolation from SEP to BIC proceeds in discrete steps as follows: For $1 \leq r \leq \lfloor n/2 \rfloor$, r many agents only value the first good, r agents value only the second good, and the remaining agents value each a separate good. One verifies that this recovers SEP for $r = 1$ and BIC for $r = \lfloor n/2 \rfloor$, and that each of these stages can be represented in the block matrix shape, where A is a column of r ones, and B is the identity matrix with possibly zero columns attached to its right. Then, $\sigma_1(A) = \sqrt{r}$ which is at least $\sigma_1(B) = 1$, which means that this interpolation step lies on the boundary. By linearly interpolating between successive steps, one obtains (after reordering) matrices of the shape

$$\left(\begin{array}{cc|cc|ccc} 1 & 0 & 0 & 0 & 0 & 0 & \cdots & 0 \\ \vdots & 0 & 0 & 0 & 0 & 0 & \cdots & 0 \\ 1 & 0 & 0 & 0 & 0 & 0 & \cdots & 0 \\ \theta & 1 - \theta & 0 & 0 & 0 & 0 & \cdots & 0 \\ \hline 0 & 0 & 1 & 0 & 0 & 0 & \cdots & 0 \\ \vdots & \vdots & \vdots & 0 & 0 & 0 & \cdots & 0 \\ 0 & 0 & 1 & 0 & 0 & 0 & \cdots & 0 \\ 0 & 0 & \theta & 1 - \theta & 0 & 0 & \cdots & 0 \\ \hline 0 & 0 & 0 & 0 & 1 & 0 & \cdots & 0 \\ 0 & 0 & 0 & 0 & 0 & 1 & \cdots & 0 \\ \vdots & \vdots & \vdots & \vdots & \vdots & \vdots & \ddots & \vdots \\ 0 & 0 & 0 & 0 & 0 & 0 & \cdots & 0 \end{array} \right),$$

which one verifies also lie on the boundary. As a result, we can continuously¹¹ interpolate from WSEP to BIC while staying on the right boundary. It follows that this interpolation traces the entire right boundary between WSEP and BIC. \square

D Additional Experimental Results

In this section, we expand upon Sections 3.2 and 4.3 by (i) presenting the remaining comparisons of the different maps for the different features, including the demand distance defined in Appendix B.2, (ii) introducing new features, and (iii) disaggregating plots of the distributions of instance sources.

¹¹While we reordered the matrix in between, this is just for exposition.

A comparison of the distance-embedding maps and the explicit map regarding the minimax envy, the maximum Nash welfare, and the maximum utilitarian welfare can be seen in Figs. 9 to 11, respectively; these show that the distance-embedding and explicit maps provide similar information regarding these features.

The same observation holds for some other features: Fig. 12 shows whether an instance permits an envy-free allocation—an information that can also be derived from the minimax envy—, while Fig. 13 shows whether an instance allows an envy-free and Pareto-efficient allocation. Interestingly, the maps of the two features look identical—indeed they are for 5×5 and 10×20 , and only differ for 15 instances for 3×6 . We have also investigated whether an instance fulfills the maximin share (MMS) criterion, which requires each agent to receive a bundle with a utility no less than the maximum, over all allocations, of the utility of the bundle with the lowest utility for the agent. We omit the corresponding maps, as each instance of our two instance set satisfies this criterion. Additionally, we investigate the fraction of the proportional share that can be guaranteed, i.e. the largest α so that $u_i(S_i) \geq \alpha \cdot \frac{u_i([m])}{n}$ for each $i \in [n]$, where S_i denotes the bundle of goods given to agent i . Across our maps shown in Figure Fig. 14, this feature follows a similar pattern as the maximum Nash welfare, which is intuitive since it is (up to scaling) the maximum achievable egalitarian welfare. Furthermore, we consider the sum, over all agents, of the maximal envies, i.e. $\sum_{i \in [n]} \max_{i' \neq i} u_i(S_{i'}) - u_i(S_i)$, which can be seen in Fig. 15 and which shows a similar color gradient to utilitarian welfare, but reversed: the sum of the maximal envies (smoothly) decreases if an instance is closer to separability.

While the previous features are based on allocations, we also consider features that can be computed solely from the utility matrix. Fig. 16 and Fig. 17 show the “maximum demand” and “preference diversity”, respectively, which are introduced in Section 4.1: These results support the correlation between the features and the singular values mentioned in the latter section. Fig. 18 shows the fraction of agents who are single-minded, i.e., who value only one item: More than half of the map is covered by instances in which at most 20% of the agents are single-minded.

In addition, we introduce the following measures: To measure the *diversity of demand*, we create a vector of all total demands and compute a Gini coefficient of this vector, where the demand for good j is defined as $\sum_{i \in [n]} u_{i,j}$. On the other hand, we compute a Gini coefficient of each vote and use the average over all votes to measure the *pickiness*. The maps showing these two features can be seen in Fig. 19 and 20 (which shows one minus pickiness, as this makes the value one for one extreme point and zero for the other extreme points, which is also the case for diversity of demand and preference diversity), which show that these measures also vary smoothly over the map.

Lastly, we highlight each of the different instance sources separately for both the 3×6 and 5×5 instances in Fig. 21 to 27—maps of the 10×20 instances are missing here, as each instance apart from the corner points are from the resampling distribution—, which show the observations about the instance sources on the distance-embedding map in Section 3.2 more clearly on both distance-embedding and explicit maps, both of which show similar distributions.

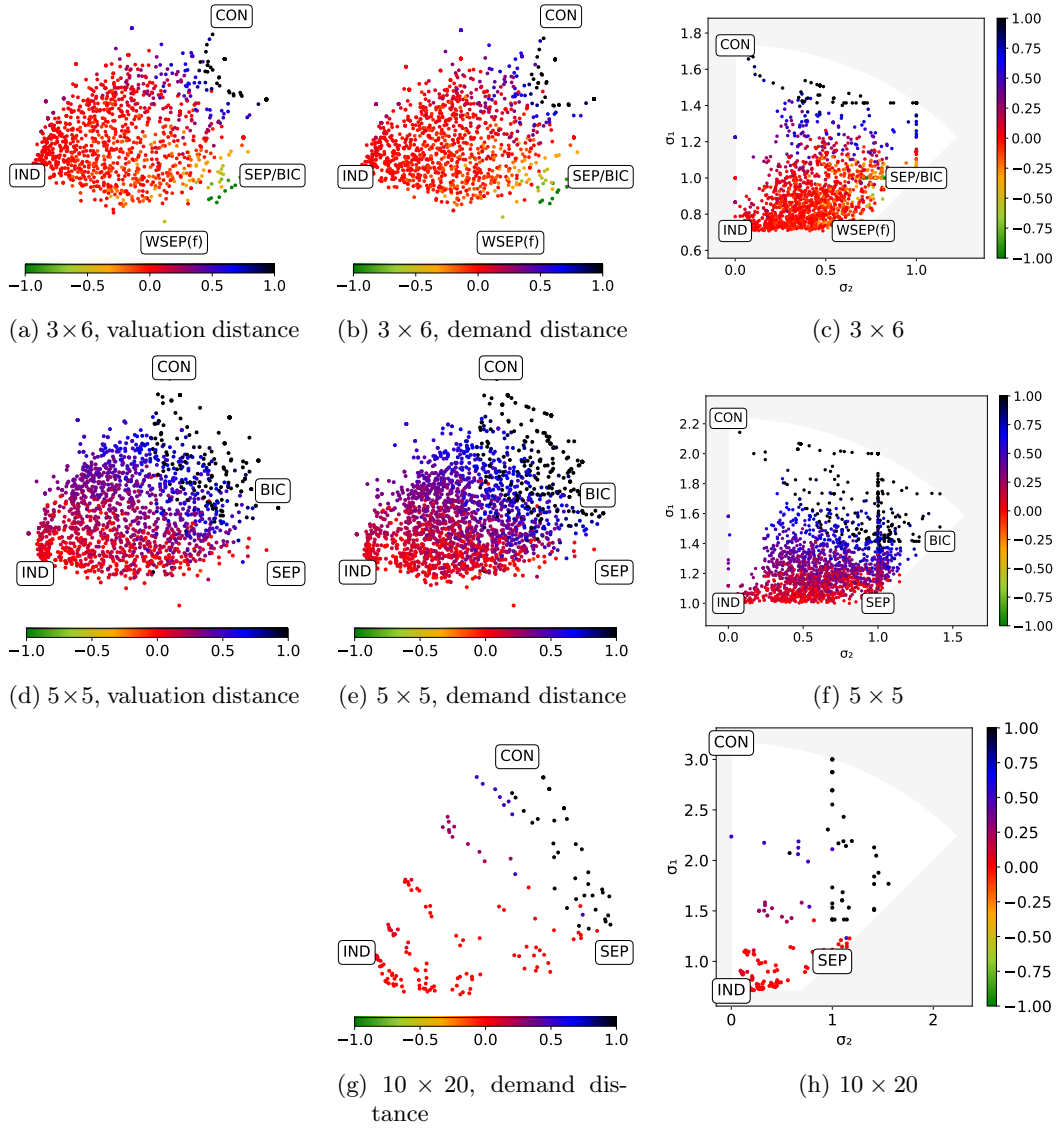


Figure 9: Distribution of the minimax envy on our distance-embedding map using the valuation distance (first column), using the demand distance (second column), and on our explicit map (third column). Computing the valuation distance for instances of the 10×20 dataset was computationally too demanding, hence the blank space in the third row.

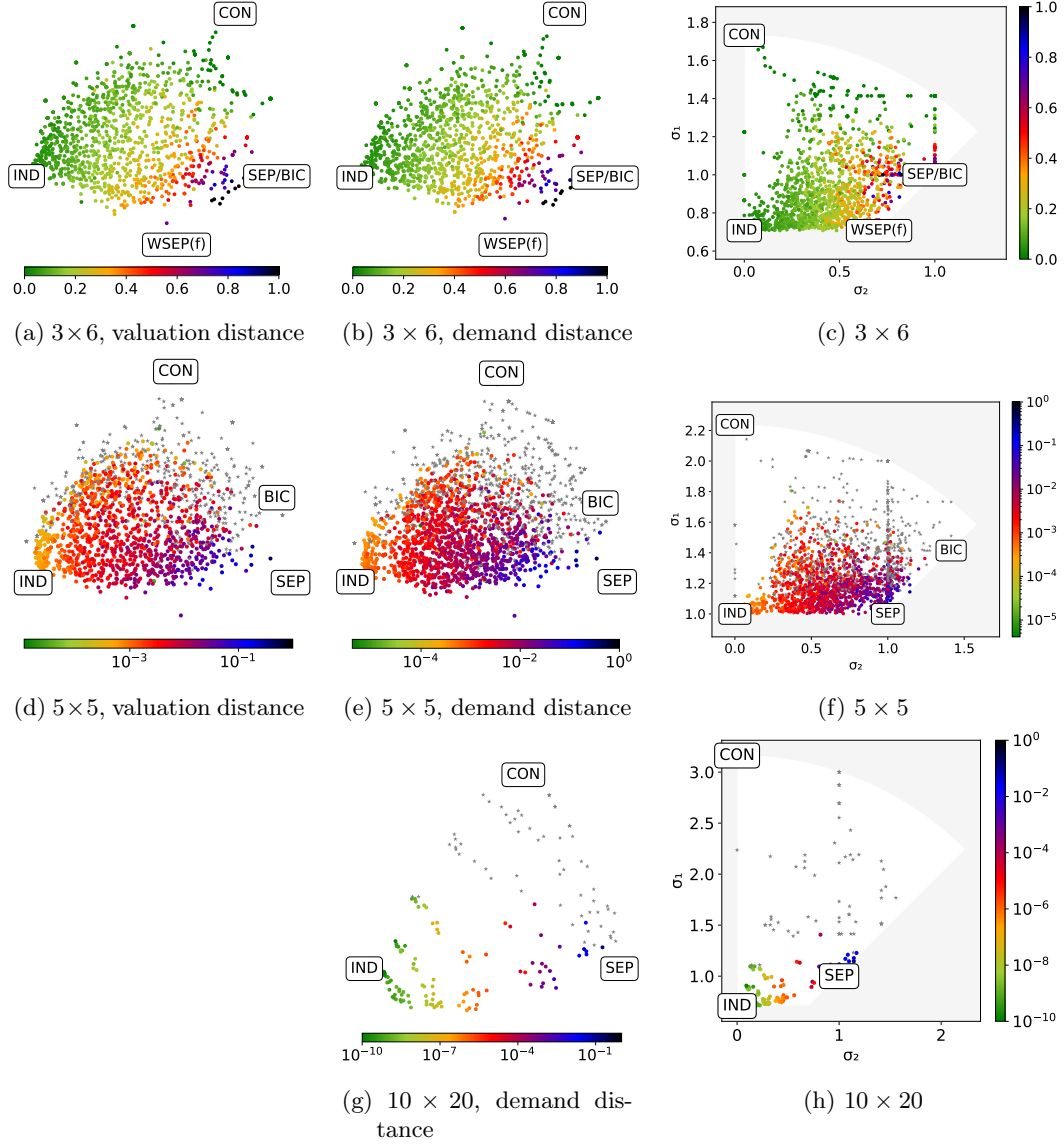


Figure 10: Distribution of the maximal Nash welfare on our distance-embedding map using the valuation distance (first column), using the demand distance (second column), and on our explicit map (third column). Grey stars represent the value 0 in the 5×5 and 10×20 maps. For the 10×20 instances, we multiply the utilities by 1000 and round them naturally while computing the allocation to avoid excessive runtimes. Computing the valuation distance for instances of the 10×20 dataset was computationally too demanding, hence the blank space in the third row.

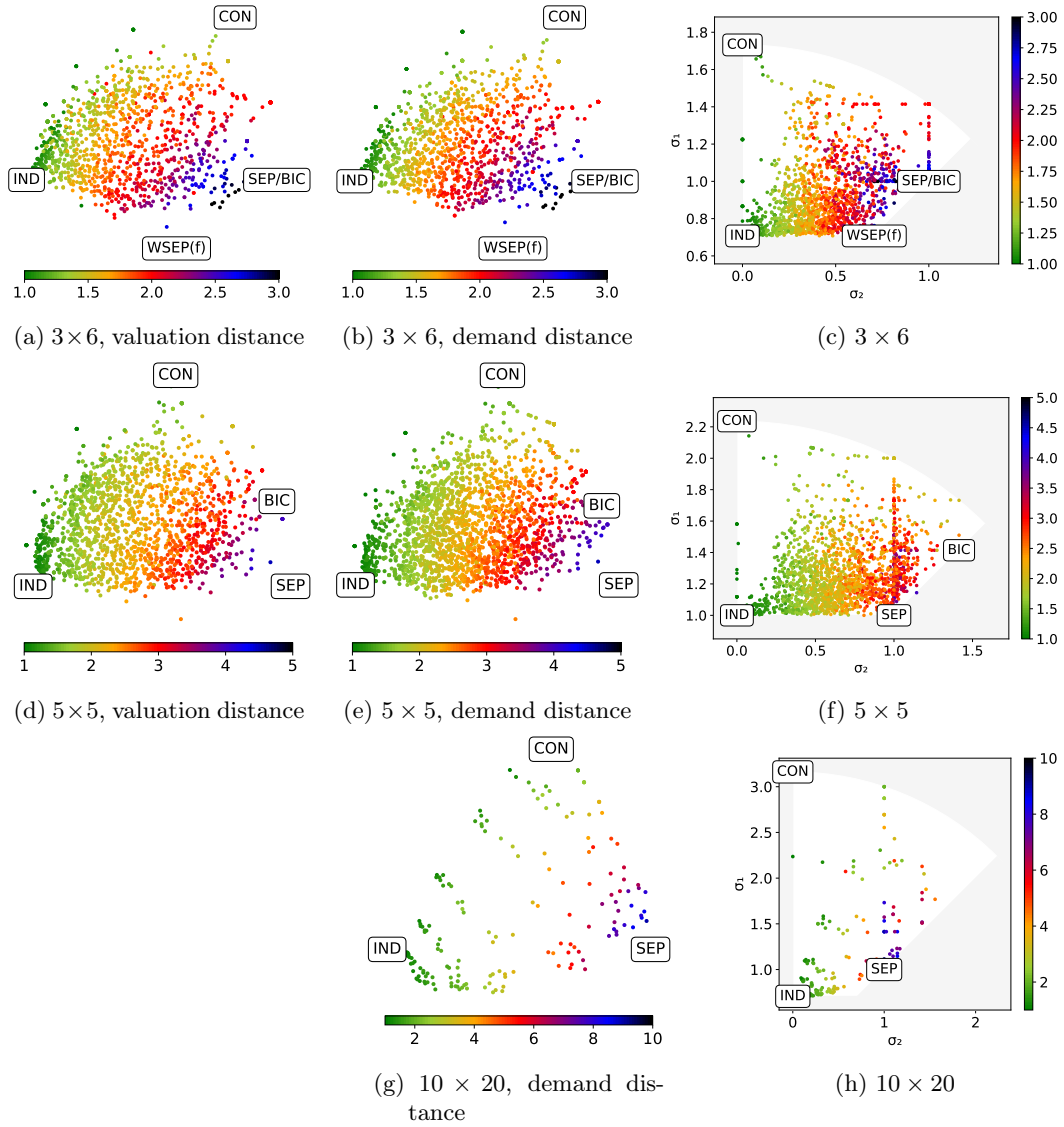


Figure 11: Distribution of the maximum utilitarian welfare on our distance-embedding map using the valuation distance (first column), using the demand distance (second column), and on our explicit map (third column). Computing the valuation distance for instances of the 10×20 dataset was computationally too demanding, hence the blank space in the third row.

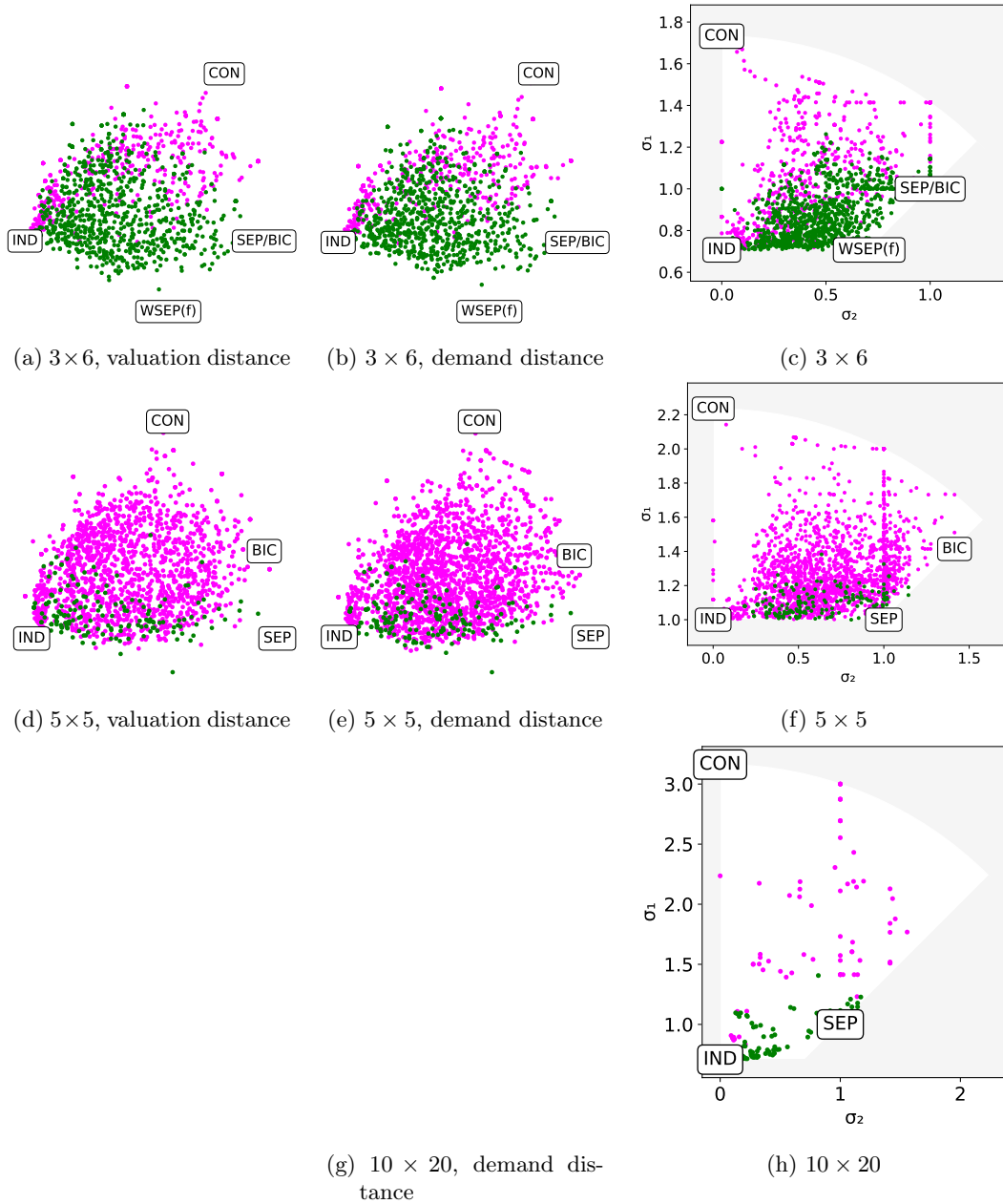


Figure 12: Distribution of the existence of an envy-free allocation on our distance-embedding map using the valuation distance (first column), using the demand distance (second column), and on our explicit map (third column). Green points indicate that an envy-free allocation exists. Computing the valuation distance for instances of the 10×20 dataset was computationally too demanding, hence the blank space in the third row.

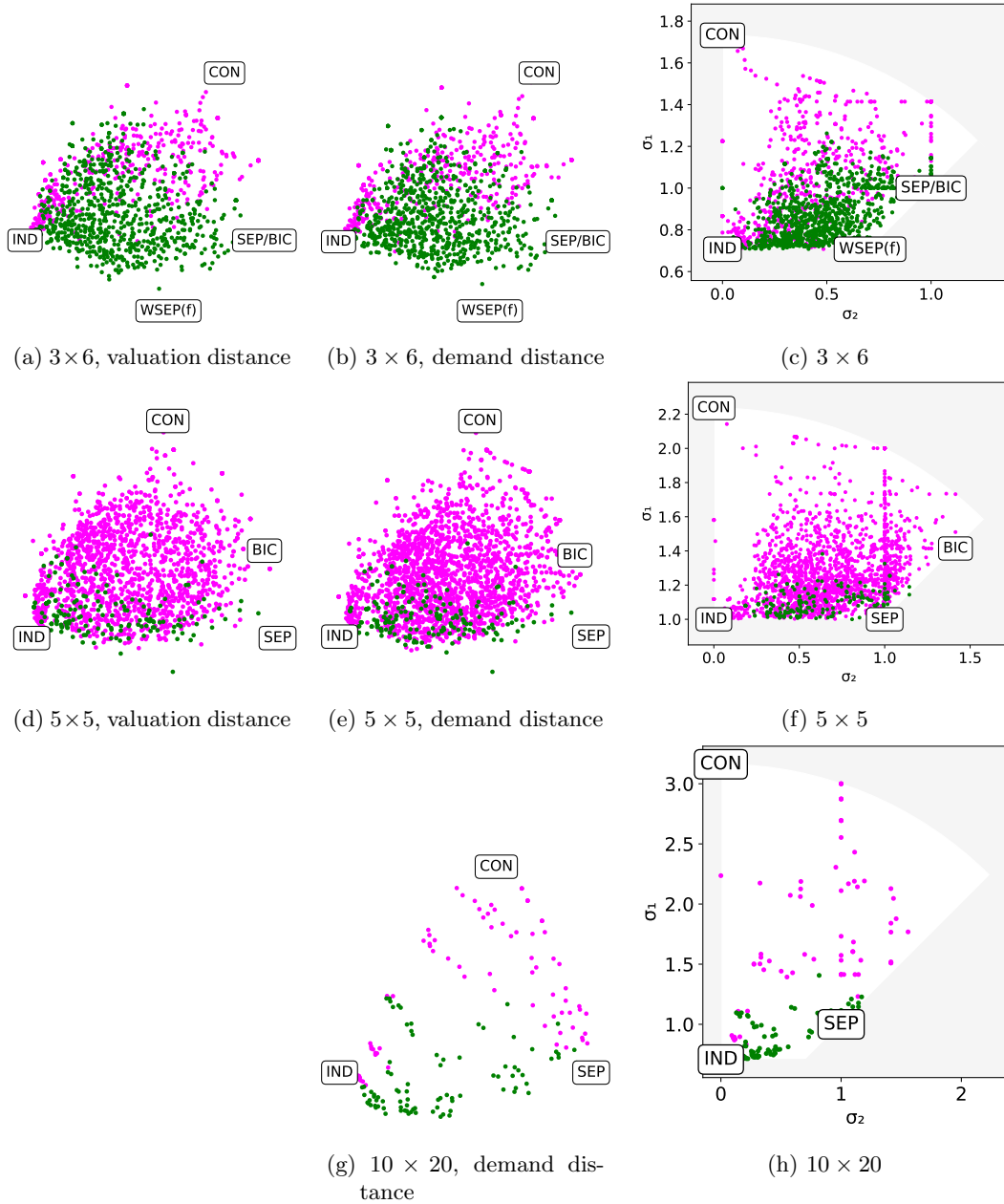


Figure 13: Distribution of the existence of an envy-free and Pareto-efficient allocation on our distance-embedding map using the valuation distance (first column), using the demand distance (second column), and on our explicit map (third column). Green points indicate that an envy-free and Pareto-efficient allocation exists. Computing the valuation distance for instances of the 10×20 dataset was computationally too demanding, hence the blank space in the third row.

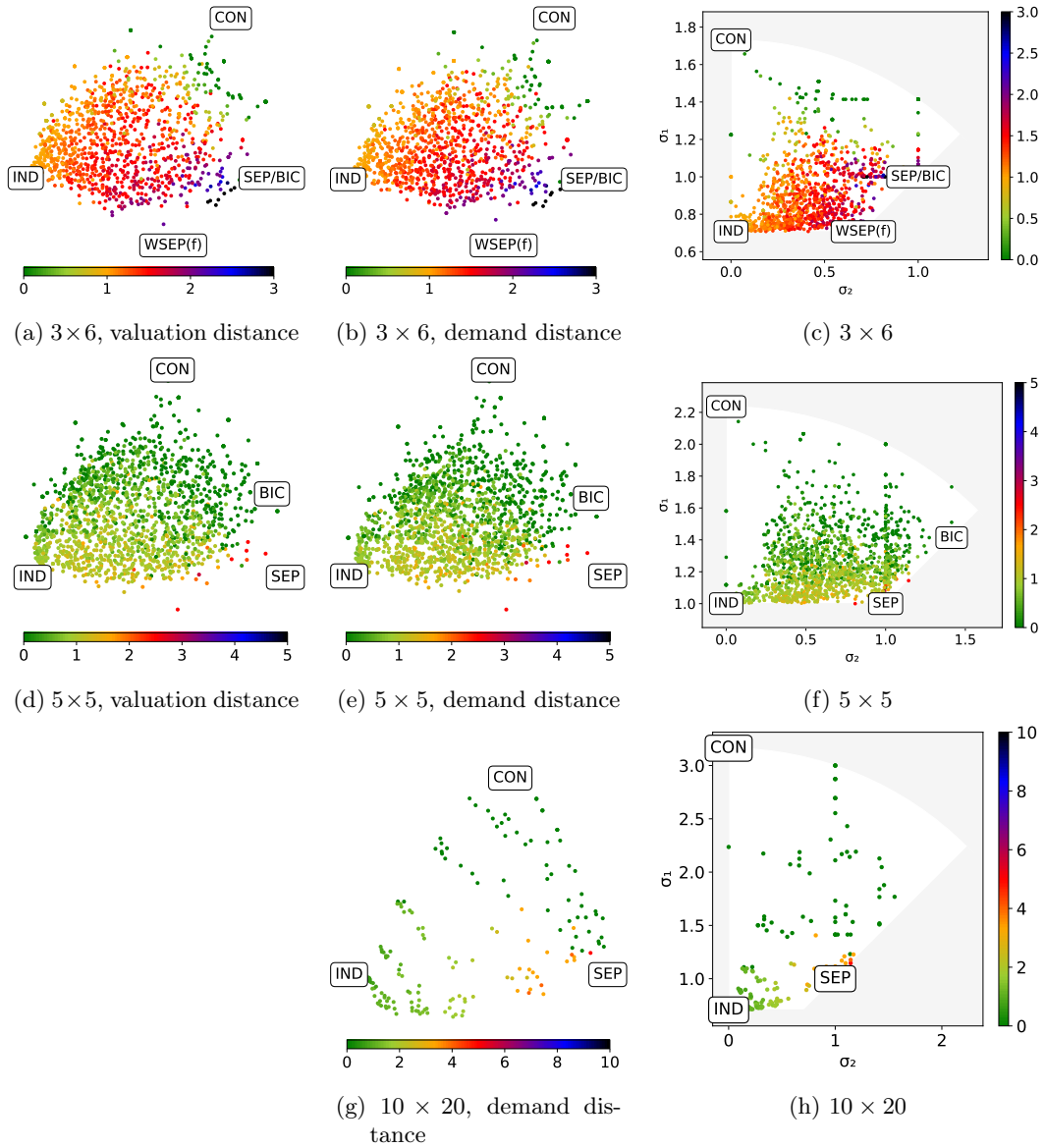


Figure 14: Distribution of fraction of the proportional share that can be guaranteed at each instance on our distance-embedding map using the valuation distance (first column), using the demand distance (second column), and on our explicit map (third column). Computing the valuation distance for instances of the 10×20 dataset was computationally too demanding, hence the blank space in the third row.

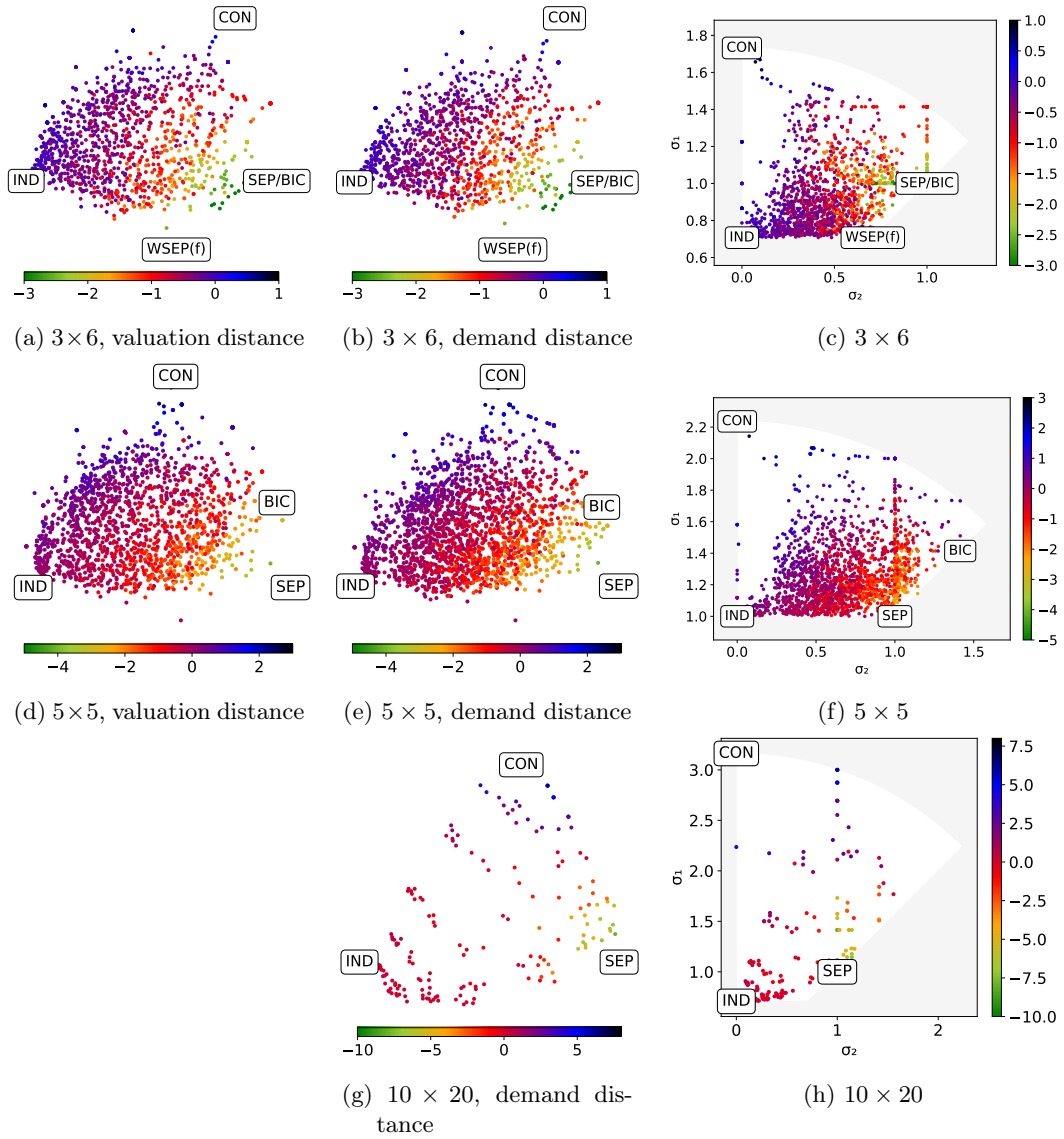


Figure 15: Distribution of the sum of the maximal envies on our distance-embedding map using the valuation distance (first column), using the demand distance (second column), and on our explicit map (third column). Computing the valuation distance for instances of the 10×20 dataset was computationally too demanding, hence the blank space in the third row.

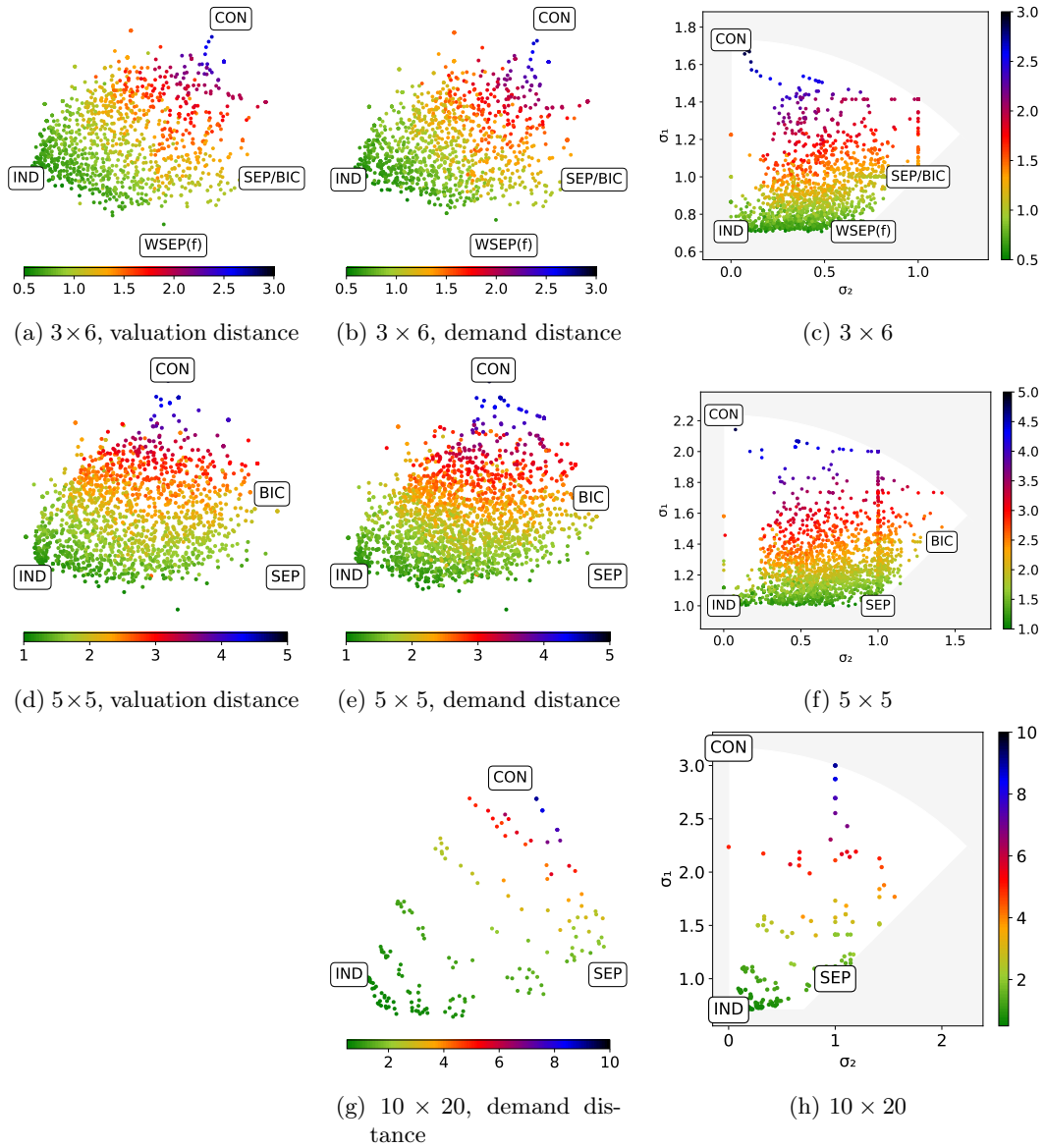


Figure 16: Distribution of the maximum demand on our distance-embedding map using the valuation distance (first column), using the demand distance (second column), and on our explicit map (third column). Computing the valuation distance for instances of the 10×20 dataset was computationally too demanding, hence the blank space in the third row.

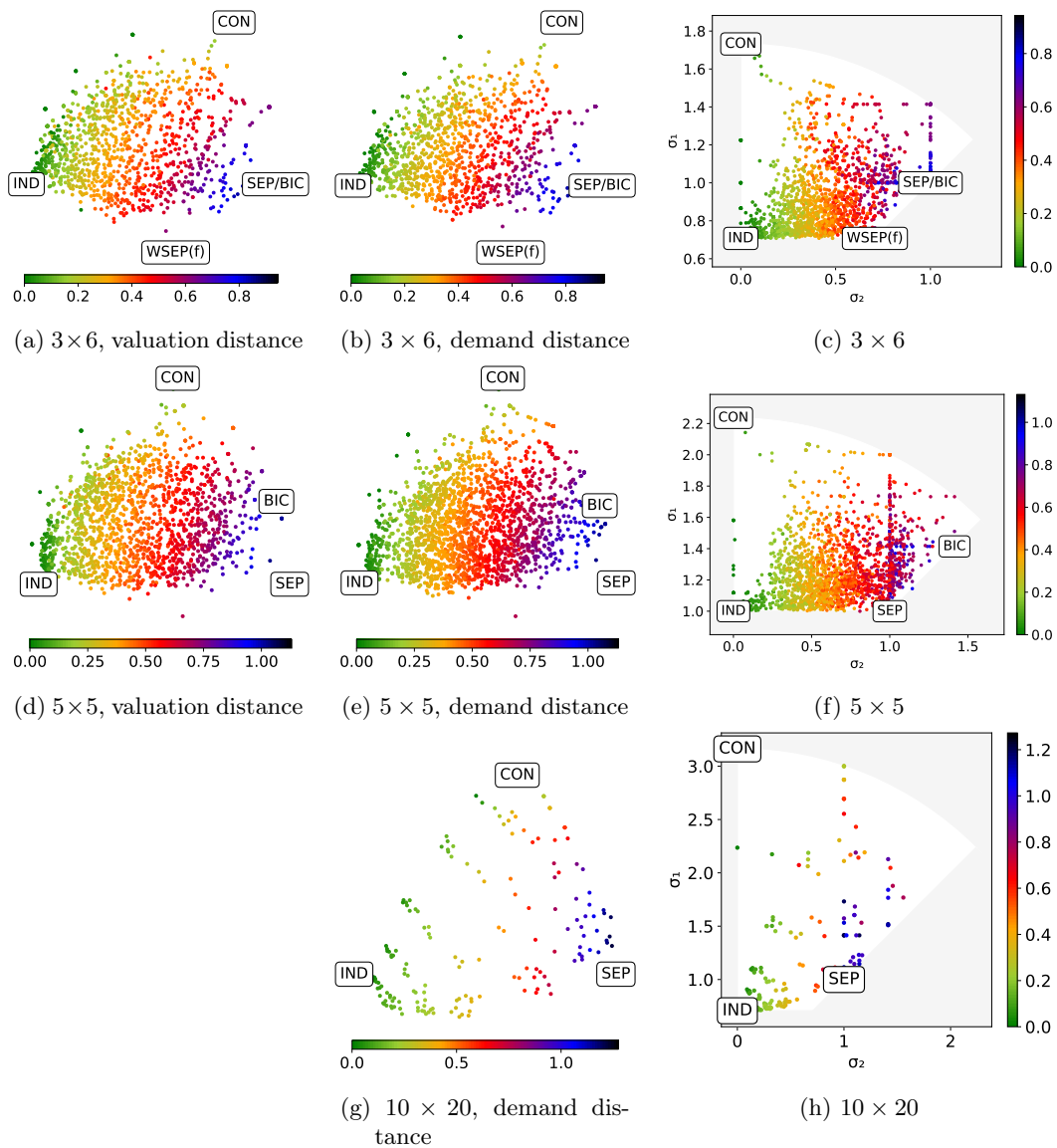


Figure 17: Distribution of the preference diversity on our distance-embedding map using the valuation distance (first column), using the demand distance (second column), and on our explicit map (third column). Computing the valuation distance for instances of the 10×20 dataset was computationally too demanding, hence the blank space in the third row.

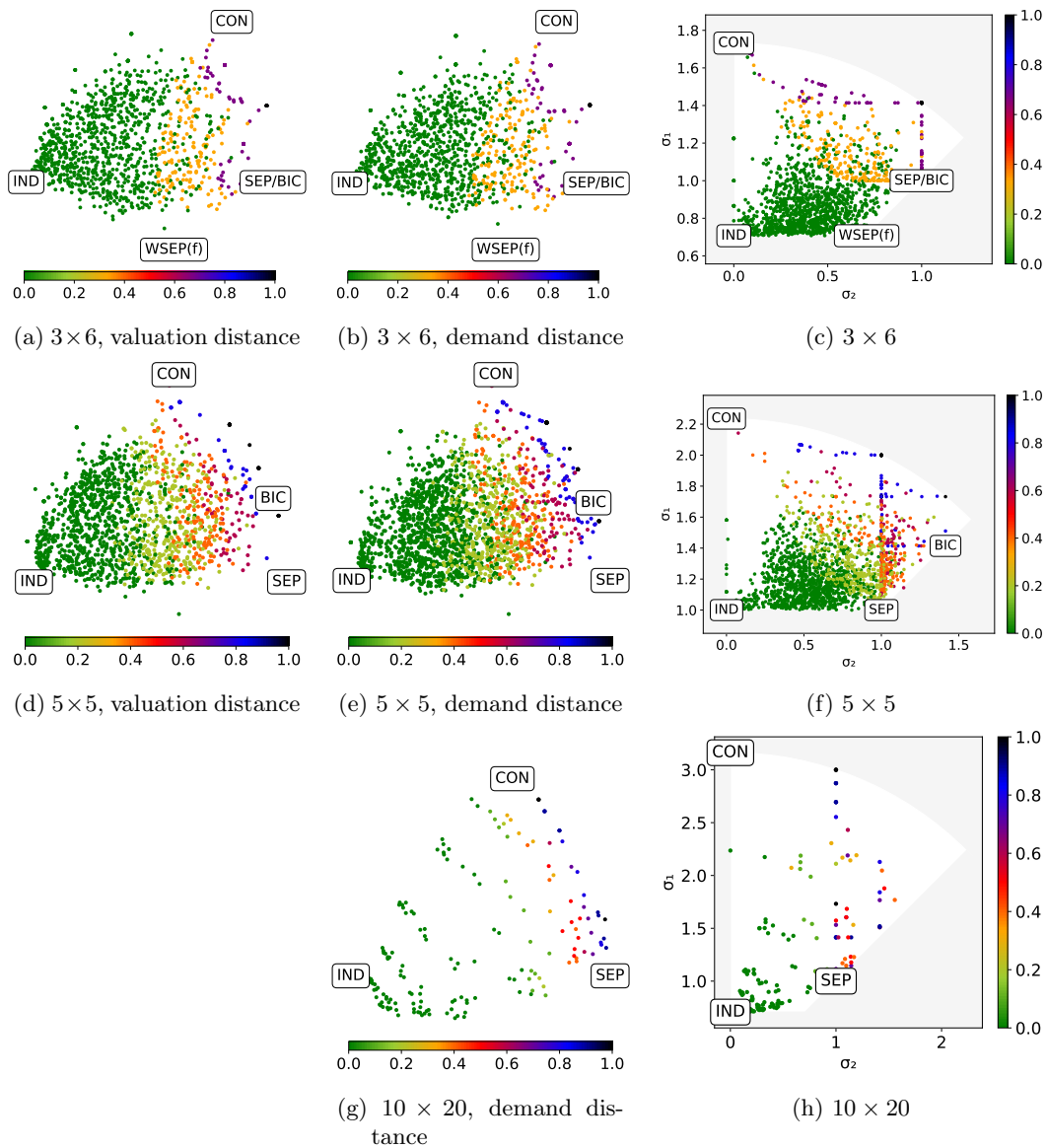


Figure 18: Distribution of the agents who are single-minded on our distance-embedding map using the valuation distance (first column), using the demand distance (second column), and on our explicit map (third column). Computing the valuation distance for instances of the 10×20 dataset was computationally too demanding, hence the blank space in the third row.

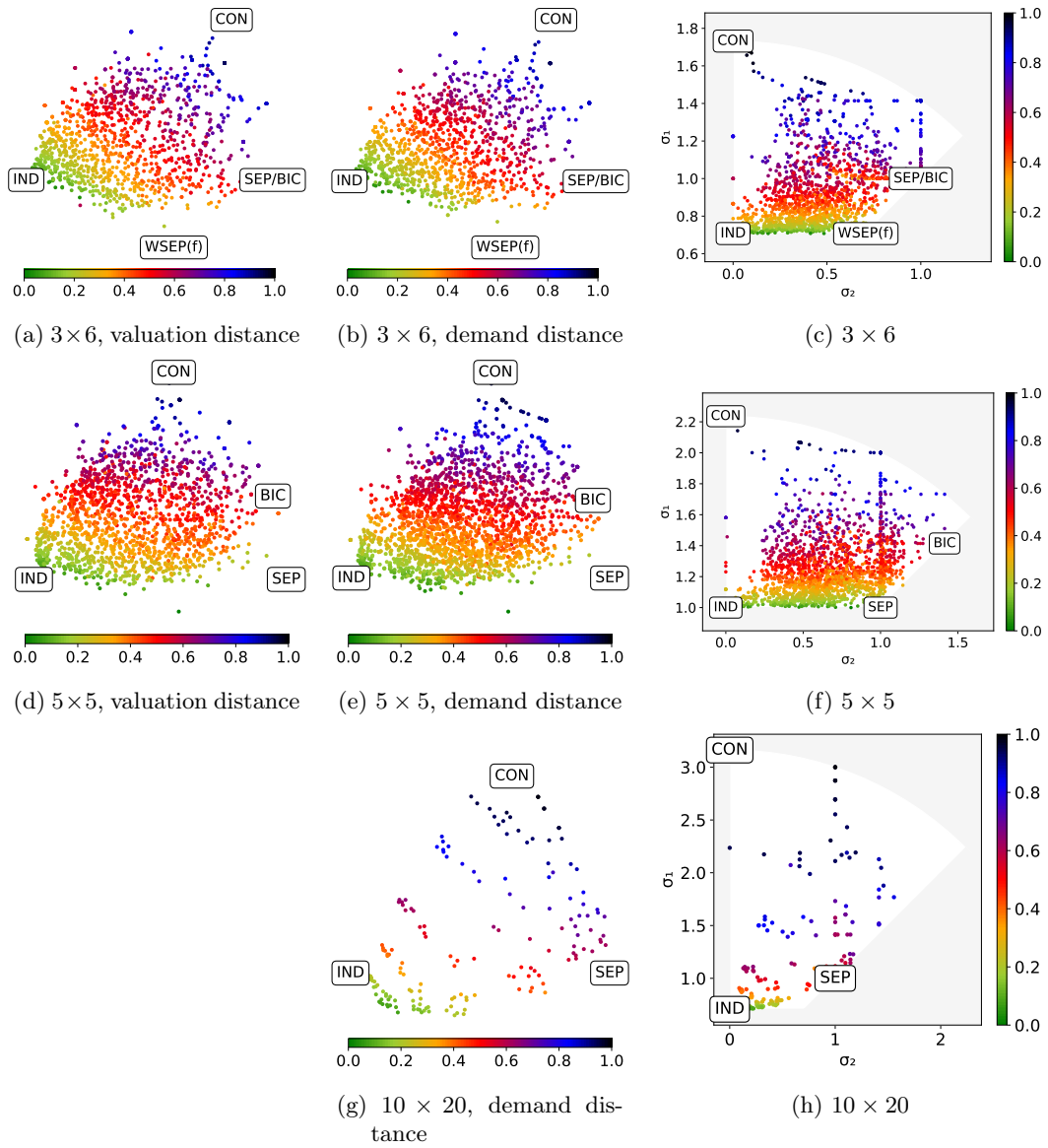


Figure 19: Distribution of the diversity of demand on our distance-embedding map using the valuation distance (first column), using the demand distance (second column), and on our explicit map (third column). Computing the valuation distance for instances of the 10×20 dataset was computationally too demanding, hence the blank space in the third row.

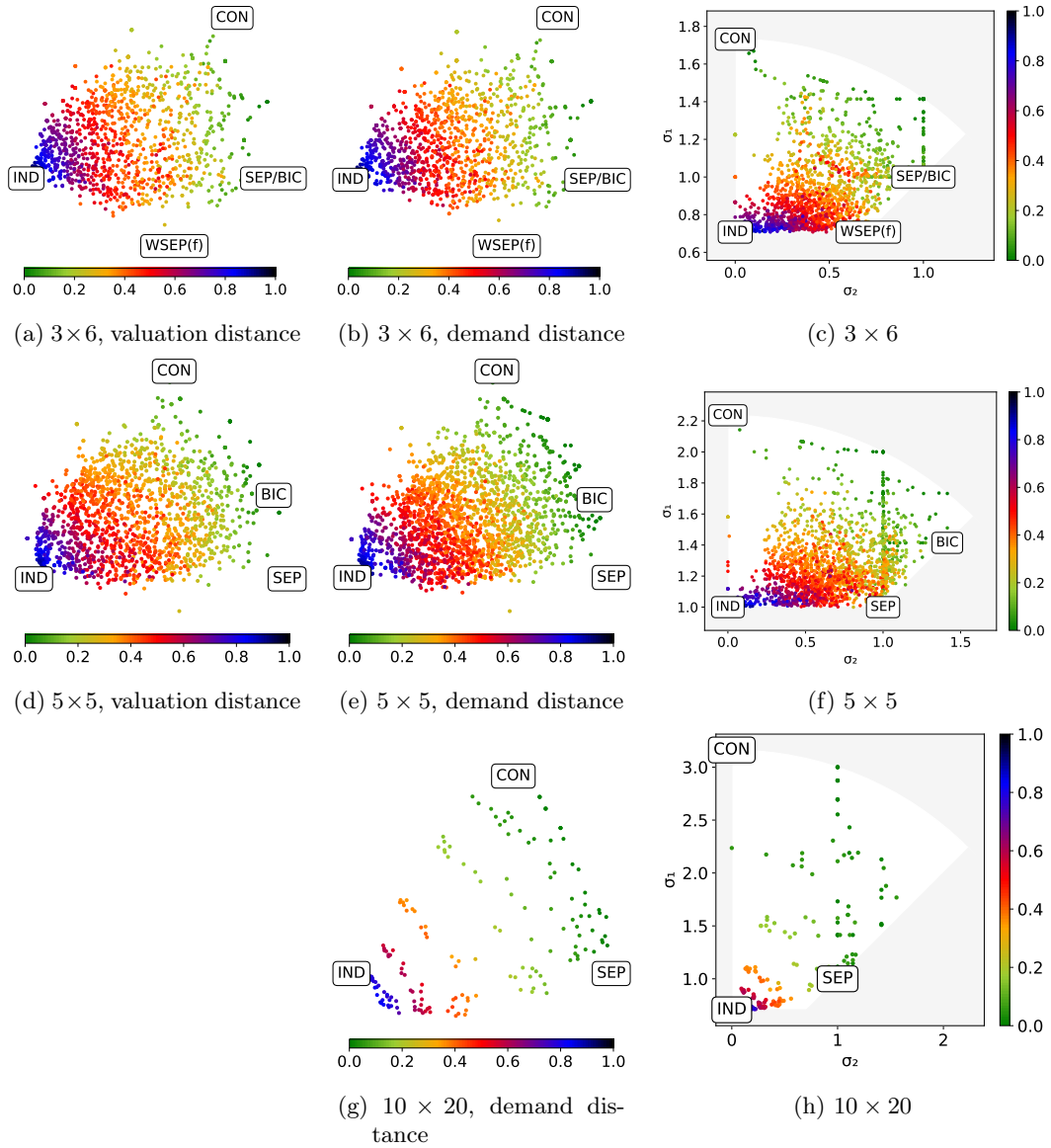


Figure 20: Distribution of one minus pickiness on our distance-embedding map using the valuation distance (first column), using the demand distance (second column), and on our explicit map (third column). Computing the valuation distance for instances of the 10×20 dataset was computationally too demanding, hence the blank space in the third row.

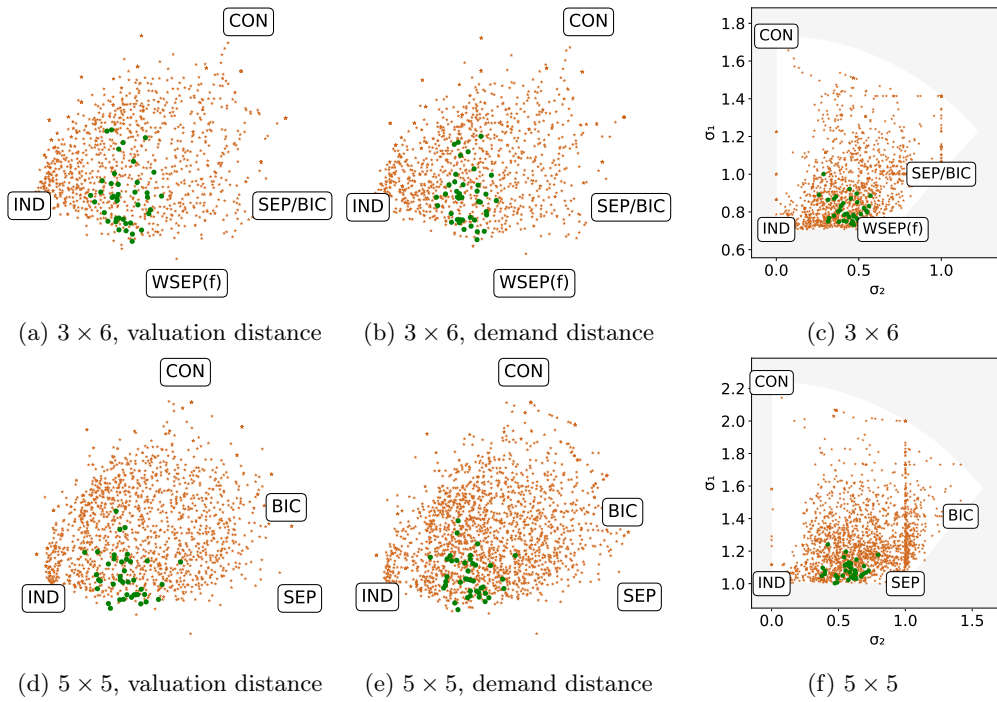


Figure 21: The instances from the i.i.d. distribution using the exponential distribution are marked as green dots, while all other instances are marked as brown stars.

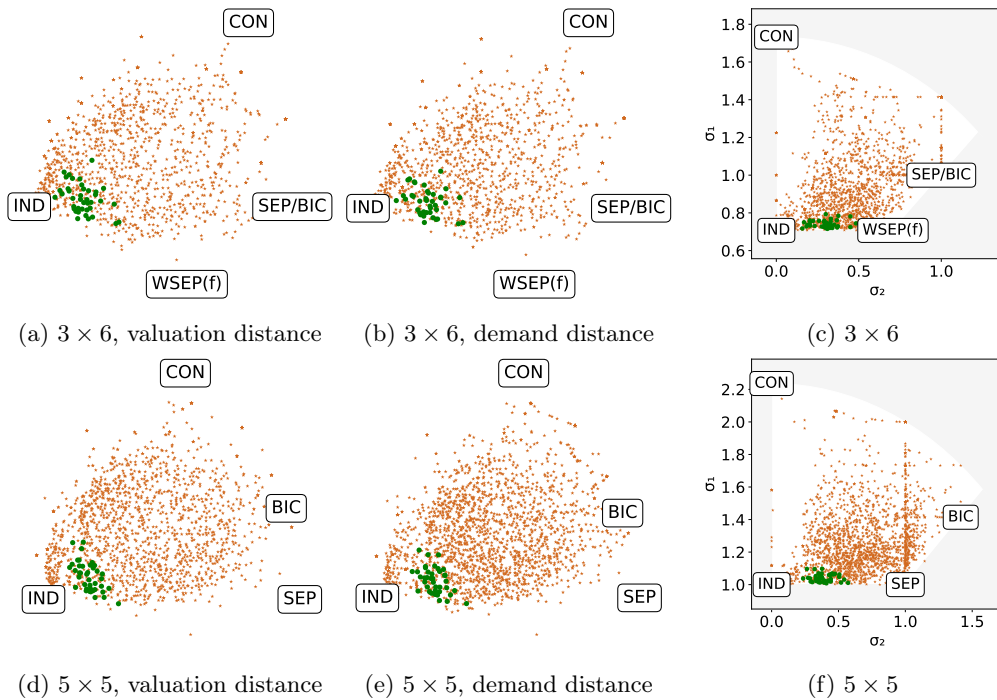


Figure 22: The instances from the i.i.d. distribution using the uniform distribution over $[0, 1]$ are marked as green dots, while all other instances are marked as brown stars.

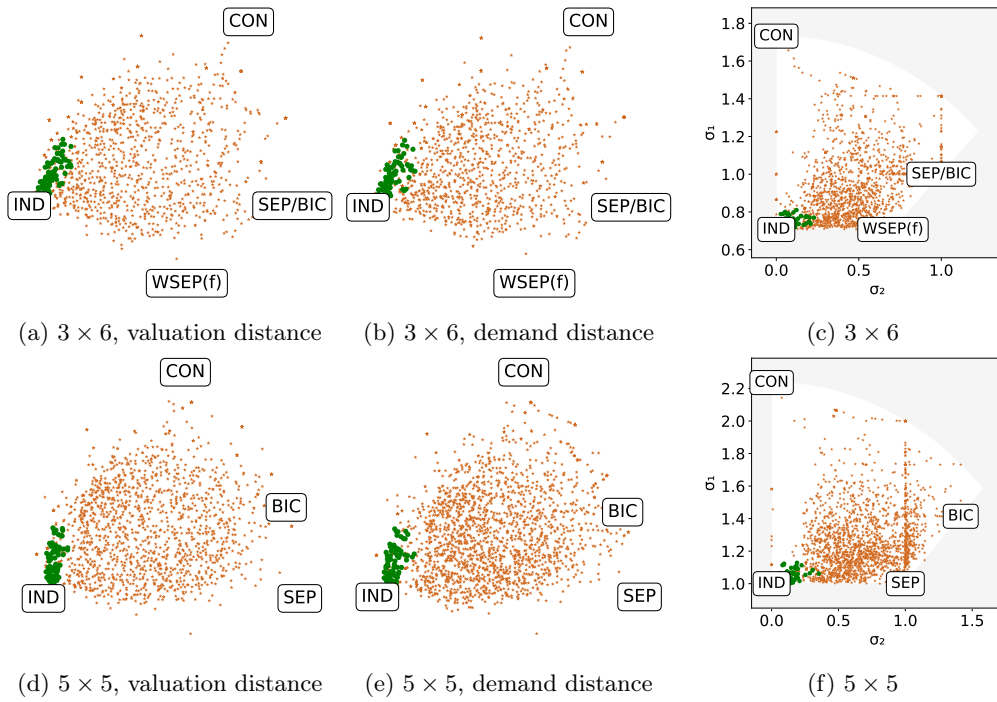


Figure 23: The instances from the attributes distribution are marked as green dots, while all other instances are marked as brown stars.

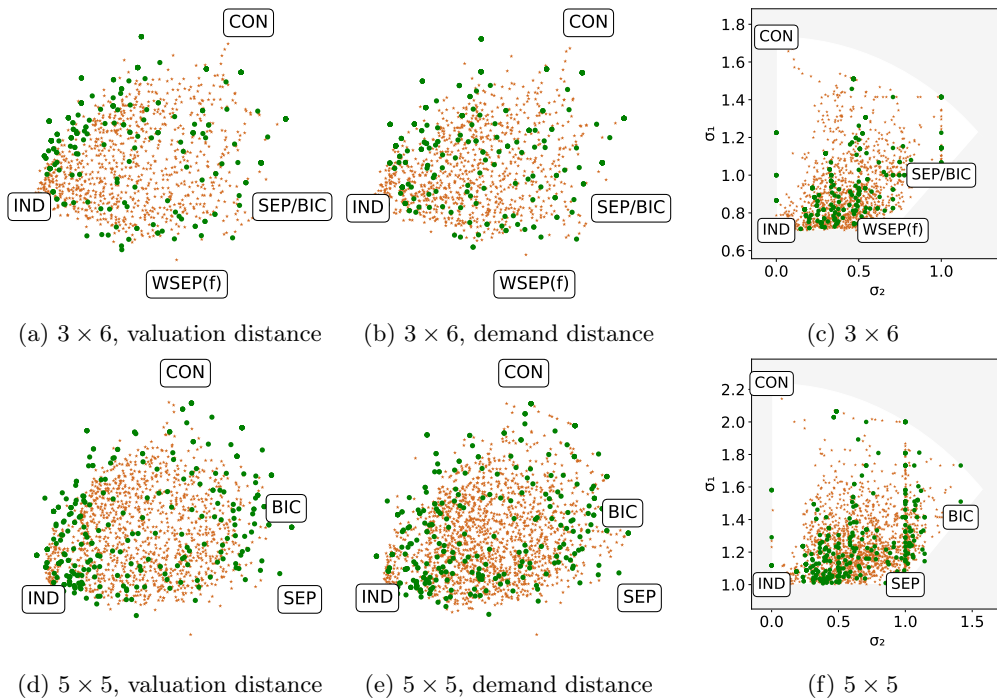


Figure 24: The instances from the resampling distribution are marked as green dots, while all other instances are marked as brown stars.

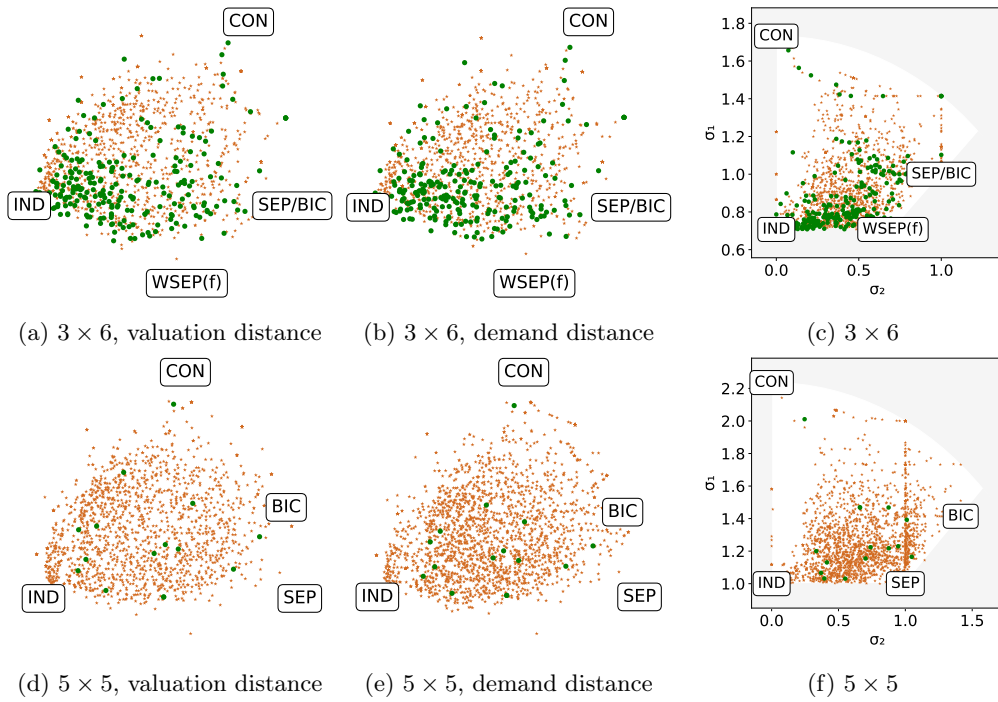


Figure 25: The instances from the Spliddit dataset are marked as green dots, while all other instances are marked as brown stars

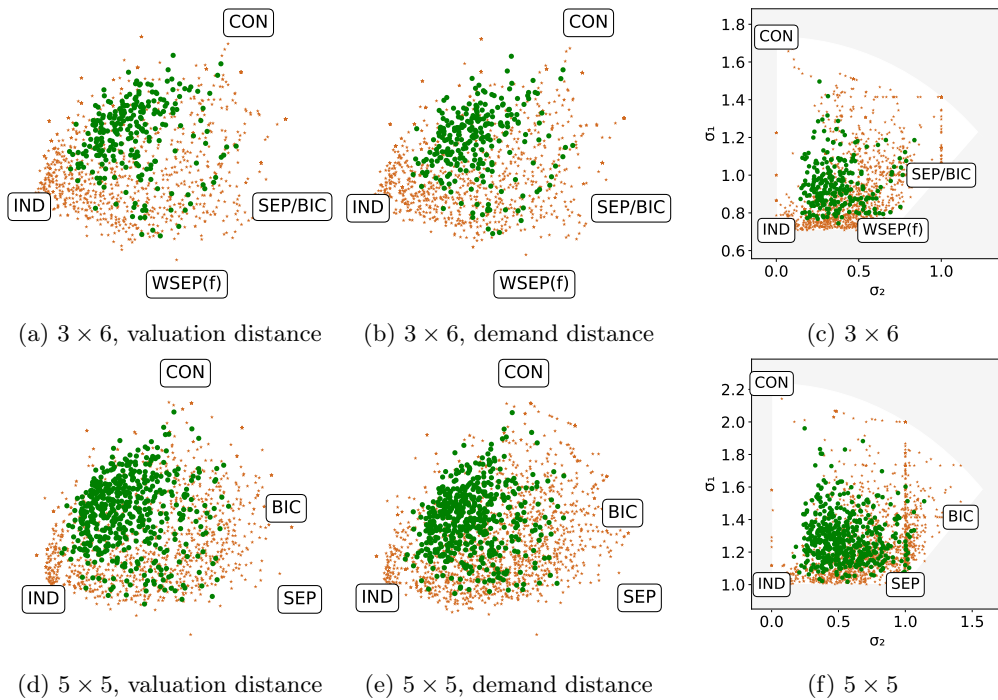


Figure 26: The instances from the island dataset are marked as green dots, while all other instances are marked as brown stars.

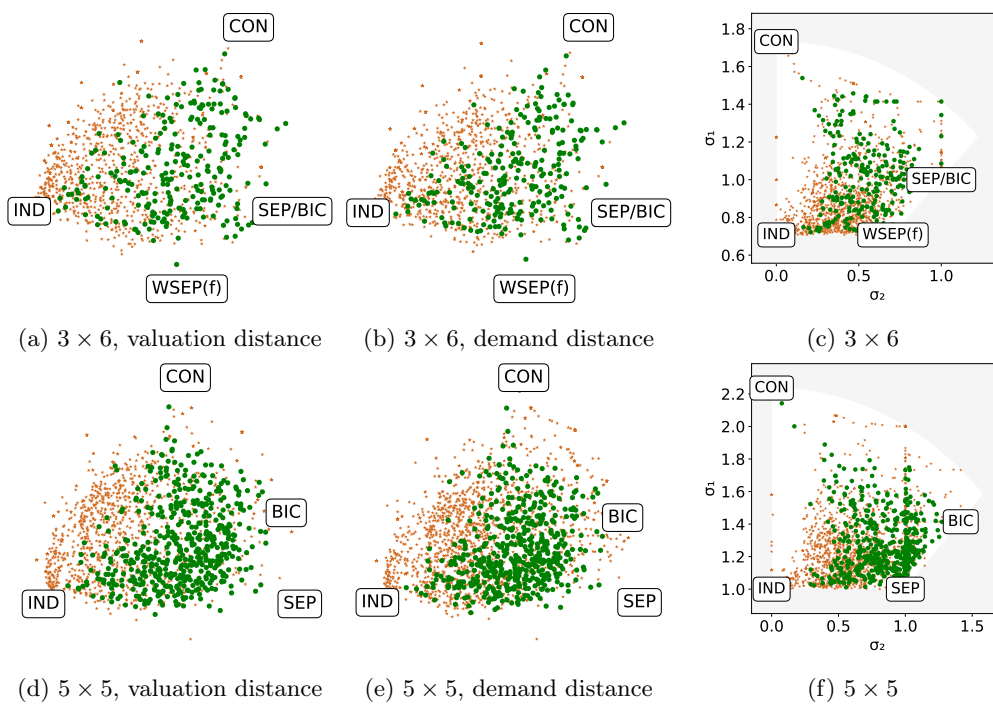


Figure 27: The instances from the candies dataset are marked as green dots, while all other instances are marked as brown stars.